arXiv:2109.00220v2 [hep-ex] 1 Dec 2021

Measurement of J/ψ production cross-sections in pp collisions at $\sqrt{s} = 5\,\text{TeV}$

LHCb collaboration[†]

Abstract

The production cross-sections of J/ψ mesons in proton-proton collisions at a centre-of-mass energy of $\sqrt{s} = 5\,\text{TeV}$ are measured using a data sample corresponding to an integrated luminosity of $9.13 \pm 0.18\,\text{pb}^{-1}$, collected by the LHCb experiment. The cross-sections are measured differentially as a function of transverse momentum, p_{T}, and rapidity, y, and separately for J/ψ mesons produced promptly and from beauty hadron decays (nonprompt). With the assumption of unpolarised J/ψ mesons, the production cross-sections integrated over the kinematic range $0 < p_{\text{T}} < 20\,\text{GeV}/c$ and $2.0 < y < 4.5$ are

$$\sigma_{\text{prompt } J/\psi} = 8.154 \pm 0.010 \pm 0.283\,\mu\text{b},$$

$$\sigma_{\text{nonprompt } J/\psi} = 0.820 \pm 0.003 \pm 0.034\,\mu\text{b},$$

where the first uncertainties are statistical and the second systematic. These cross-sections are compared with those at $\sqrt{s} = 8\,\text{TeV}$ and $13\,\text{TeV}$, and are used to update the measurement of the nuclear modification factor in proton-lead collisions for J/ψ mesons at a centre-of-mass energy per nucleon pair of $\sqrt{s_{\text{NN}}} = 5\,\text{TeV}$. The results are compared with theoretical predictions.

[†]Authors are listed at the end of this paper.

1 Introduction

Quantum chromodynamics (QCD) is the fundamental theory that describes the strong interaction between quarks and gluons. One of the most important properties of QCD is that the coupling constant increases at small momentum transfers. Non-perturbative corrections, which are challenging to control theoretically, are required to describe many observables. The study of heavy quarkonium production in proton-proton (pp) collisions can provide important information to improve QCD predictions in the non-perturbative regime. The process involves the production of a $Q\overline{Q}$ system, where Q denotes a beauty or charm quark, followed by its hadronisation into the heavy quarkonium state. Predictions based on the assumption of factorisation have been found to agree well with experimental data so far. The $Q\overline{Q}$ production step can be calculated with perturbative QCD but the hadronisation step, being of non-perturbative nature, needs to be described by models with inputs from experiments. The colour singlet model [1–7] assumes that the intermediate $Q\overline{Q}$ state is colourless and has the same spin-parity quantum numbers as the quarkonium state. In the nonrelativistic QCD (NRQCD) approach [8–10] intermediate $Q\overline{Q}$ states with all possible colour and spin-parity quantum numbers may evolve into a quarkonium state. The transition probabilities are described by long-distance matrix elements (LDME) that cannot be calculated perturbatively and are therefore determined from experimental data.

In pp collisions J/ψ mesons can be produced either directly from hard collisions of partons, through the feed-down of excited charmonium states, or via decays of beauty hadrons. The J/ψ mesons from the first two sources originate from the primary pp collision vertex (PV) and are called *prompt* J/ψ mesons, while those from the last source originate from decay vertices of beauty hadrons, which are typically separated from the PV, and are called *nonprompt* J/ψ mesons. The differential cross-sections for prompt and nonprompt J/ψ mesons in pp collisions were measured in the rapidity range $2.0 < y < 4.5$ by the LHCb collaboration at centre-of-mass energies of $\sqrt{s} = 2.76$ TeV [11], 7 TeV [12], 8 TeV [13] and 13 TeV [14]. They were also measured by the ATLAS collaboration at $\sqrt{s} = 5$ TeV [15], 7 TeV [16], 8 TeV [16] and 13 TeV [17] in the region $|y| < 2$, and by the CMS collaboration at $\sqrt{s} = 5$ TeV [18] and 7 TeV [19, 20] in the region $|y| < 2.4$. Prompt J/ψ production cross-sections were measured by the CMS collaboration at $\sqrt{s} = 13$ TeV [21] in the region $|y| < 1.2$ and by the ALICE collaboration at $\sqrt{s} = 7$ TeV [22] in the region $|y| < 0.9$. The measurements for inclusive J/ψ mesons, which include both prompt and nonprompt contributions, were also performed by the ALICE collaboration at $\sqrt{s} = 2.76$ TeV [23], 5 TeV [24, 25] and 7 TeV [26] in the regions $|y| < 0.9$ and $2.5 < y < 4.0$, and at $\sqrt{s} = 8$ TeV [27] and 13 TeV [28] in the region $2.5 < y < 4.0$. In addition, the CDF experiment measured the prompt and nonprompt J/ψ cross-sections in proton-antiproton collisions at $\sqrt{s} = 1.8$ TeV [29] and 1.96 TeV [30]. The D0 experiment measured the inclusive J/ψ cross-sections in proton-antiproton collisions at $\sqrt{s} = 1.8$ TeV [31, 32].

This paper reports a J/ψ cross-section measurement in pp collisions at $\sqrt{s} = 5$ TeV using a data sample collected by the LHCb experiment, corresponding to an integrated luminosity of $9.13 \pm 0.18 \, \text{pb}^{-1}$ [33]. This data sample was taken with special runs for cross-section measurements. The measurement includes the production cross-sections of prompt and nonprompt J/ψ mesons with transverse momentum $p_{\text{T}} < 20 \, \text{GeV}/c$ and rapidity $2.0 < y < 4.5$, assuming unpolarised J/ψ mesons, and the cross-section ratios between 8 TeV and 5 TeV and between 13 TeV and 5 TeV. The nuclear modification factor for J/ψ mesons in pPb collisions at $\sqrt{s_{\text{NN}}} = 5$ TeV, which was originally published in

Ref. [34], is updated using the pp cross-sections reported in here.

2 Detector and simulation

The LHCb detector [35, 36] is a single-arm forward spectrometer covering the pseudorapidity range $2 < \eta < 5$, designed for the study of particles containing b or c quarks. The detector includes a high-precision tracking system consisting of a silicon-strip vertex detector surrounding the pp interaction region, a large-area silicon-strip detector located upstream of a dipole magnet with a bending power of about $4\,\mathrm{Tm}$, and three stations of silicon-strip detectors and straw drift tubes placed downstream of the magnet. The tracking system provides a measurement of the momentum, p, of charged particles with a relative uncertainty that varies from 0.5% at low momentum to 1.0% at $200\,\mathrm{GeV}/c$. The minimum distance of a track to a primary pp collision vertex, the impact parameter (IP), is measured with a resolution of $(15 + 29/p_\mathrm{T})\,\mathrm{\mu m}$, where p_T is in GeV/c. Different types of charged hadrons are distinguished using information from two ring-imaging Cherenkov detectors. Photons, electrons and hadrons are identified by a calorimeter system consisting of scintillating-pad (SPD) and preshower detectors, an electromagnetic and a hadronic calorimeter. Muons are identified by a system composed of alternating layers of iron and multiwire proportional chambers. The online event selection is performed by a trigger, which consists of a hardware stage, based on information from the calorimeter and muon systems, followed by a software stage, which applies a full event reconstruction.

Simulated events are required to determine corrections for the detector resolution, acceptance and efficiency. The pp collisions are modelled using PYTHIA [37, 38] with a specific LHCb configuration [39]. In the PYTHIA model, J/ψ mesons are generated with zero polarisation and the leading order colour-singlet and colour-octet contributions [39, 40] are considered in prompt J/ψ production. Decays of unstable particles are described by EVTGEN [41] with QED final-state radiation handled by PHOTOS [42]. The interactions of the generated particles with the detector are modelled using the GEANT4 toolkit [43, 44] as described in Ref. [45].

3 Selection of J/ψ candidates

The J/ψ candidates are reconstructed through the $J/\psi \to \mu^+\mu^-$ decay channel and are selected through two trigger stages. The hardware trigger selects events with at least one muon candidate with $p_\mathrm{T} > 900\,\mathrm{MeV}/c$. The software trigger requires two loosely identified muons, having $p_\mathrm{T} > 500\,\mathrm{MeV}/c$ and $p > 3000\,\mathrm{MeV}/c$, to form a good-quality vertex. In the offline selection the muon identification requirement is tightened and both tracks are required to have $p_\mathrm{T} > 650\,\mathrm{MeV}/c$ and $2.0 < \eta < 4.9$. The background from fake tracks is reduced by a neural-network based algorithm [46]. The invariant mass of each J/ψ candidate, $m_{\mu^+\mu^-}$, is required to be within a range of $\pm 120\,\mathrm{MeV}/c^2$ around the known J/ψ mass [47]. All events are required to have at least one reconstructed PV. For candidates with multiple PVs in the event, the one with the smallest χ^2_IP is taken as the associated PV, where χ^2_IP is defined as the difference in the vertex-fit χ^2 of a given PV reconstructed with and without the J/ψ candidate under consideration.
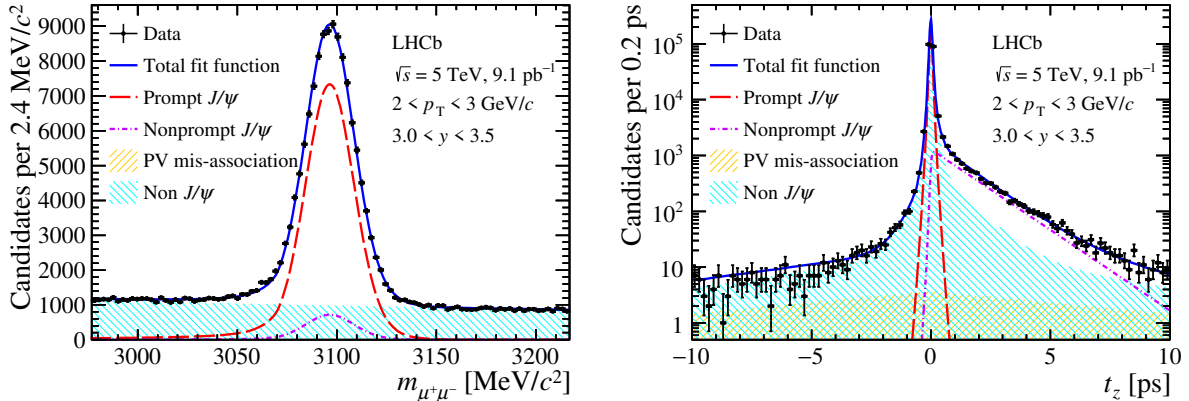
Figure 1: Distributions of (left) invariant mass and (right) pseudoproper time of the J/ψ candidate for an example interval corresponding to $2 < p_{\mathrm{T}} < 3 \,\mathrm{GeV}/c$ and $3.0 < y < 3.5$. Projections of the two-dimensional fit are also shown.

A final selection is applied to J/ψ candidates using the pseudoproper time t_z, defined as

$$t_z = \frac{z_{J/\psi} - z_{\mathrm{PV}}}{p_z} \times m_{J/\psi}, \qquad (1)$$

where $z_{J/\psi}$ and z_{PV} are positions the J/ψ decay vertex and the PV along the beam axis z, p_z is the projection of the measured momentum of the J/ψ candidate along the z axis, and $m_{J/\psi}$ is the known J/ψ mass [47]. The t_z uncertainty σ_{t_z} is calculated by combining the estimated uncertainties on the z position of the J/ψ decay vertex and that of the associated PV. Candidates with $|t_z| < 10\,\mathrm{ps}$ and $\sigma_{t_z} < 0.3\,\mathrm{ps}$ are selected for further analysis.

4 Cross-section determination

The double-differential cross-section of J/ψ production in a given (p_{T}, y) interval is defined as

$$\frac{\mathrm{d}^2\sigma}{\mathrm{d}p_{\mathrm{T}}\mathrm{d}y} = \frac{N(J/\psi \to \mu^+\mu^-)}{\mathcal{L} \times \varepsilon_{\mathrm{tot}} \times \mathcal{B} \times \Delta p_{\mathrm{T}} \times \Delta y}, \qquad (2)$$

where $N(J/\psi \to \mu^+\mu^-)$ is the signal yield, $\varepsilon_{\mathrm{tot}}$ is the detection efficiency, $\mathcal{L}$ is the integrated luminosity, $\mathcal{B} = (5.961 \pm 0.033)\%$ [47] is the branching fraction of the $J/\psi \to \mu^+\mu^-$ decay, and Δp_{T} and Δy are the interval widths. Details on the interval scheme are provided in Sec. 6.

The yields of prompt and nonprompt J/ψ mesons are simultaneously extracted from an unbinned extended maximum-likelihood fit to the two-dimensional distribution of $m_{\mu^+\mu^-}$ and t_z independently in each (p_{T}, y) interval. The total J/ψ signal yield is about 1.4 (0.14) million for prompt (nonprompt) J/ψ mesons. Figure 1 shows the projections of the two-dimensional distribution, together with the fit, on $m_{\mu^+\mu^-}$ and t_z for one (p_{T}, y) interval. There are four components: prompt J/ψ signal, nonprompt J/ψ signal, J/ψ signal with incorrect PV association, and non-J/ψ background from random tracks. The first three J/ψ signals have the same mass shape but their t_z distributions are different.

3

In each interval the mass shape of J/ψ signals is described by the sum of two Crystal Ball (CB) functions [48] with a common mean value and independent widths. The simulation is used to determine the values of the two power-law tail parameters, which are shared between the two CB functions and fixed in the fit. Only the mean and widths of the CB functions and the ratio between the two functions are left as free shape parameters in the fit. The mass distribution of the non-J/ψ background is modelled with an exponential function.

The true t_z values for prompt J/ψ mesons are assumed to be zero while those for nonprompt J/ψ mesons are assumed to follow an exponential function. These distributions are convolved with the sum of two Gaussian functions to model the t_z resolution. The two Gaussian functions share the same mean value and their widths are proportional to the t_z uncertainty σ_{t_z}. The J/ψ signal with incorrect PV association contributes to the long tail present in the t_z distribution. This component can be modelled from data using event mixing, $i.e.$, calculating t_z with the J/ψ candidate associated to the closest PV in the next event of the sample. The yield of this component is divided into two parts, $N_{\mathrm{p}}^{\mathrm{tail}}$ and $N_{\mathrm{np}}^{\mathrm{tail}}$, according to the ratio between prompt and nonprompt yields, and then $N_{\mathrm{p}}^{\mathrm{tail}}$ and $N_{\mathrm{np}}^{\mathrm{tail}}$ are added to the prompt and nonprompt yields respectively. The t_z distribution of the non-J/ψ background is described by an empirical function composed of a delta function and five exponential functions that are convolved with the sum of two Gaussian resolution functions sharing the same mean value. All parameters of the empirical function are fixed to the values obtained from a fit to the t_z distribution of the J/ψ mass sidebands, defined by the region $75 < |m_{\mu^+\mu^-} - m_{J/\psi}| < 150 \, \mathrm{MeV}/c^2$.

The detection efficiency is determined in each (p_{T},y) interval using simulated samples. The distribution of the number of SPD hits in simulation is weighted to match that in data to correct the effect of the detector occupancy in simulation. The efficiency $\varepsilon_{\mathrm{tot}}$ is factorised into the product of four efficiencies: the acceptance, $\varepsilon_{\mathrm{acc}}$, the reconstruction-and-selection efficiency, $\varepsilon_{\mathrm{rec\&sel}}$, the particle identification (PID) efficiency, $\varepsilon_{\mathrm{PID}}$, and the trigger efficiency, $\varepsilon_{\mathrm{tri}}$. The efficiencies $\varepsilon_{\mathrm{acc}}$ and $\varepsilon_{\mathrm{rec\&sel}}$ are evaluated separately for prompt and nonprompt J/ψ mesons. The efficiencies $\varepsilon_{\mathrm{PID}}$ and $\varepsilon_{\mathrm{tri}}$ are calculated combining the simulated samples of prompt and nonprompt J/ψ mesons, as the differences between the two production processes are observed to be negligible. The efficiency $\varepsilon_{\mathrm{tri}}$ is validated using data, and the efficiencies of track reconstruction and PID obtained from simulation are corrected using control channels in data, as detailed in Sec. 5.

5 Systematic uncertainties

A summary of systematic uncertainties is presented in Table 1. Uncertainties arising from signal extraction and efficiency determination are mostly evaluated in each (p_{T},y) interval, while those due to branching fraction and luminosity measurement are common to all intervals. The details of the evaluation are discussed in the following.

An uncertainty is attributed to the choice of the probability density function used to model the dimuon invariant-mass distribution of the signal components. As an alternative to the sum of two CB functions, the signal invariant-mass distribution is described by a model derived from simulation using the approach of kernel density estimation [49]. To account for the resolution difference between data and simulation, the alternative model is convolved with a Gaussian function with zero mean and width varied freely. The default

and alternative model are compared in each (p_{T},y) interval and the relative difference, which is up to 2.0%, is taken as a systematic uncertainty.

The exponential function describing the background is replaced by a linear function and the relative difference, varying up to 0.7%, is taken as a systematic uncertainty. The resulting uncertainty is considered as fully correlated between intervals.

The t_z model used for the description of the non-J/ψ background is replaced by the use of the *sPlot* method [50] using the $m_{\mu^+\mu^-}$ as the discriminating variable. The relative difference between the two methods varies up to 1.2% for prompt and 4.0% for nonprompt J/ψ mesons in different intervals.

An uncertainty is attributed to the method that is used to separate prompt and nonprompt J/ψ mesons, *i.e.*, two-dimensional fits to $m_{\mu^+\mu^-}$ and t_z distributions. To evaluate this uncertainty in each (p_{T},y) interval, the same t_z probability density function is used to fit the simulation. While the relative differences between the fitted and the true yields are small for most intervals, they are significant for nonprompt J/ψ mesons in a few small-p_{T} intervals. These differences, varying up to 0.8% for prompt and 14.7% for nonprompt J/ψ mesons, are taken as systematic uncertainties, and are assumed to be fully correlated between p_{T} intervals and uncorrelated between y intervals as indicated by simulation.

A systematic uncertainty related to the tracking efficiency is evaluated as follows. The efficiency correction factors are obtained from dedicated data and simulation samples of $J/\psi \to \mu^+\mu^-$ decays in which one muon track is fully reconstructed and the other track is reconstructed using a subset of tracking systems [51]. These correction factors are found to depend on different event multiplicity variables. This introduces a systematic uncertainty of 0.8% per track. The statistical uncertainties on these factors are propagated to the systematic uncertainties of the cross-sections, which vary up to 3.7% depending on the (p_{T},y) interval.

The PID efficiency is evaluated using a dedicated sample of $J/\psi \to \mu^+\mu^-$ candidates in which only one track is required to be identified as a muon. The uncertainties of the muon identification efficiencies due to the finite size of the calibration data sample are propagated to the systematic uncertainties of the cross-sections, which are up to 2.2% in different intervals. Another uncertainty comes from the choice of interval scheme of the calibration sample. The resulting uncertainties vary up to 1.5% depending on the (p_{T},y) interval.

The trigger efficiency in simulation is validated with data. One muon is requested to pass the hardware-trigger requirement such that the other muon can be regarded as an unbiased probe of the efficiency of one muon. The hardware-trigger efficiency of the J/ψ candidate is the probability that at least one muon track passes the trigger requirement. The relative difference between data and simulation, varying up to 1.9% across intervals, is taken as a systematic uncertainty on the hardware-trigger efficiency. The software-trigger efficiency is determined using a subset of events that would pass the trigger requirement if the J/ψ signals were excluded [52]. The fraction of J/ψ candidates for which two tracks pass the software-trigger requirement is taken as the efficiency both for data and simulation. The overall relative difference between data and simulation is 1.0%, and is taken as a systematic uncertainty on the software-trigger efficiency common to all intervals.

The statistical uncertainties of the efficiencies due to the finite size of the simulated sample result in uncertainties on the cross-sections. The values range up to 3.7% for

Table 1: Relative systematic uncertainties on the measurement of the J/ψ production cross-section. The symbol $\oplus$ means addition in quadrature. The detailed uncertainties for each (p_T,y) interval are in Appendix A.

Source	Relative uncertainty	Correlations
Signal mass model	$< 2.0\%$	Uncorrelated
Background mass model	$< 0.7\%$	Correlated between intervals
Background t_z model	$< 1.2\%$ (prompt) $< 4.0\%$ (nonprompt)	Uncorrelated
Signal t_z model	$< 0.8\%$ (prompt) $< 14.7\%$ (nonprompt)	Correlated between p_T intervals
Tracking efficiency	$(2 \times 0.8\%) \oplus (< 3.7\%)$	Correlated between intervals
PID efficiency	$(< 2.2\%) \oplus (< 1.5\%)$	Correlated between intervals
Hardware-trigger efficiency	$< 1.9\%$	Correlated between intervals
Software-trigger efficiency	1.0%	Correlated between intervals
Simulation sample size	$< 3.7\%$ (prompt) $< 7.7\%$ (nonprompt)	Uncorrelated
$\mathcal{B}(J/\psi \to \mu^+\mu^-)$	0.6%	Correlated between intervals
Luminosity	2.0%	Correlated between intervals
Radiative tail	1.0%	Correlated between intervals

prompt and 7.7% for nonprompt J/ψ mesons depending on the (p_T,y) interval.

The uncertainty on the $J/\psi \to \mu^+\mu^-$ branching fraction [47] results in an uncertainty on the measured cross-sections of 0.6%. The luminosity is determined using methods similar to those described in Ref. [33] and the relative uncertainty is 2.0%. The tail shape on the left side of the CB function is used to describe the effect of QED radiation, which leads to energy loss in some J/ψ candidates. A small fraction of the J/ψ signal lies outside the mass range of the fit. This signal loss is taken into account in the efficiency $\varepsilon_{\mathrm{rec\&sel}}$ estimated with the simulated sample. The imperfect modelling of the radiative decay is considered as a source of systematic uncertainty. Based on a detailed comparison between the radiative tails in simulation and data a systematic uncertainty of 1.0% is assigned.

6 Production cross-sections results

The measured double-differential cross-sections for prompt and nonprompt J/ψ mesons are shown in Fig. 2 and listed in Tables 2 and 3 in Appendix A, for the range $0 < p_\mathrm{T} < 14\,\mathrm{GeV}/c$ and $2.0 < y < 4.5$ with Δp_T between 1 and $4\,\mathrm{GeV}/c$ and $\Delta y = 0.5$. By integrating the double-differential results over p_T or y, the single-differential cross-sections $\mathrm{d}\sigma/\mathrm{d}p_\mathrm{T}$ and $\mathrm{d}\sigma/\mathrm{d}y$ are obtained, and are listed in Tables 4, 5, 6 and 7 in Appendix A. The $\mathrm{d}\sigma/\mathrm{d}p_\mathrm{T}$ results include a further p_T interval in the range $14 < p_\mathrm{T} < 20\,\mathrm{GeV}/c$, which is not divided into y intervals due to the limited size of the data sample. The integrated cross-sections for prompt and nonprompt J/ψ mesons in the range $0 < p_\mathrm{T} < 20\,\mathrm{GeV}/c$ and $2.0 < y < 4.5$ are

$$\sigma_{\mathrm{prompt}\ J/\psi} = 8.154 \pm 0.010 \pm 0.283\,\mu\mathrm{b},$$
$$\sigma_{\mathrm{nonprompt}\ J/\psi} = 0.820 \pm 0.003 \pm 0.034\,\mu\mathrm{b},$$
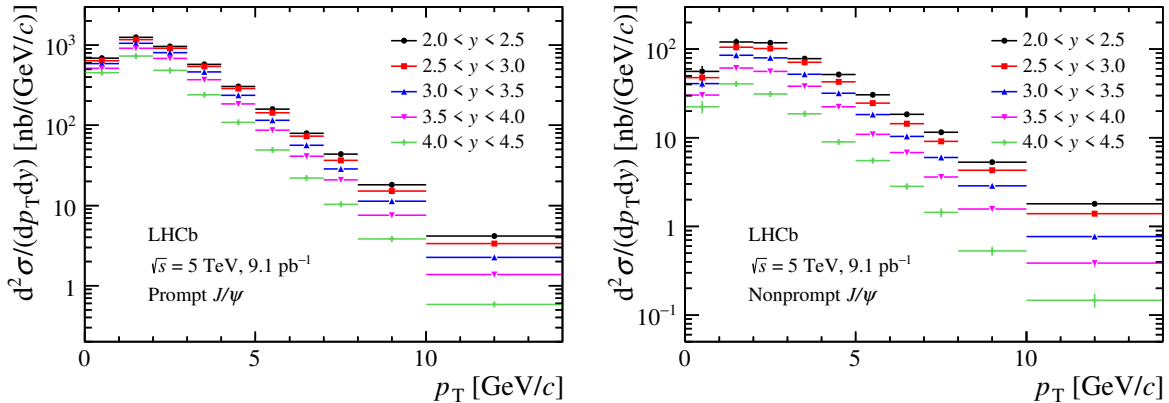
Figure 2: Differential cross-sections for (left) prompt and (right) nonprompt J/ψ mesons as a function of p_T in intervals of y. The error bars represent the total uncertainties, which are partially correlated between intervals.

where the first uncertainties are statistical and the second systematic. These results are obtained under the assumption that the polarisation of the J/ψ mesons is negligible. The J/ψ polarisation measurement at $\sqrt{s} = 7\,\mathrm{TeV}$ [53] indicates that the polarisation parameters λ_θ, $\lambda_{\theta\phi}$ and λ_ϕ are consistent with zero while the central value of λ_θ is around -0.2 in the helicity frame. The polarisation affects the detection efficiency and the dependence of the cross-sections on the polarisation is reported in Appendix B. When the polarisation parameter λ_θ is assumed to be -0.2 [53], the total cross-section decreases by 2.8% (2.9%) for prompt (nonprompt) J/ψ mesons.

The single-differential cross-sections for prompt J/ψ mesons are compared with NRQCD calculations and colour glass condensate (CGC) effective theory results, as shown in Fig. 3. Theoretical calculations in the high p_T region are obtained from the NLO NRQCD model with LDMEs fixed from the Tevatron data [54], and those in the low-p_T region are obtained by combining the NRQCD model with CGC effective theory [55], in which nonperturbative parameters are fixed by fits to the Tevatron [56] and HERA [57] data. Uncertainties due to LDMEs determination, renormalisation scales, and factorisation scales are considered for the NRQCD and CGC calculations.

A comparison between single-differential cross-sections for nonprompt J/ψ mesons and fixed order plus next-to-leading logarithms (FONLL) calculations [58,59] is shown in Fig. 4. The FONLL approach provides cross-sections for b-quark production, and the branching fraction of the decay $b \to J/\psi X$, $(1.16\pm0.10)\%$ [47], is taken from measurements performed in e^+e^- collisions at LEP. The FONLL calculations take into account the uncertainties of parton distribution functions (PDFs), the uncertainty due to the b-quark mass, and that due to the scales of renormalisation and factorisation. The total uncertainty of FONLL is dominated by the latter source.

The fraction of nonprompt J/ψ mesons is defined as the ratio between the nonprompt cross-section and the sum of prompt and nonprompt cross-sections, and the results in (p_T, y) intervals are shown in Fig. 5 and Table 8 in Appendix A. Most systematic uncertainties cancel in the ratio. Only the uncertainties due to the t_z fit and the size of simulated sample are included. The fraction increases as a function of p_T. For a given p_T, the fraction decreases with increasing y.
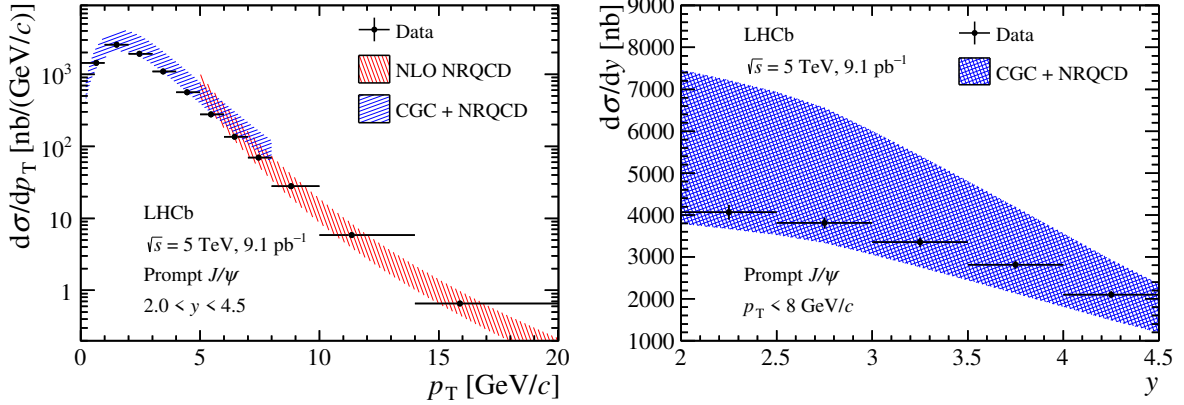
Figure 3: Differential cross-sections (left) $d\sigma/dp_T$ and (right) $d\sigma/dy$ for prompt J/ψ mesons compared with NRQCD and CGC calculations [54, 55]. Uncertainties due to LDMEs determination, renormalisation scales, and factorisation scales are included in the NRQCD and CGC predictions.
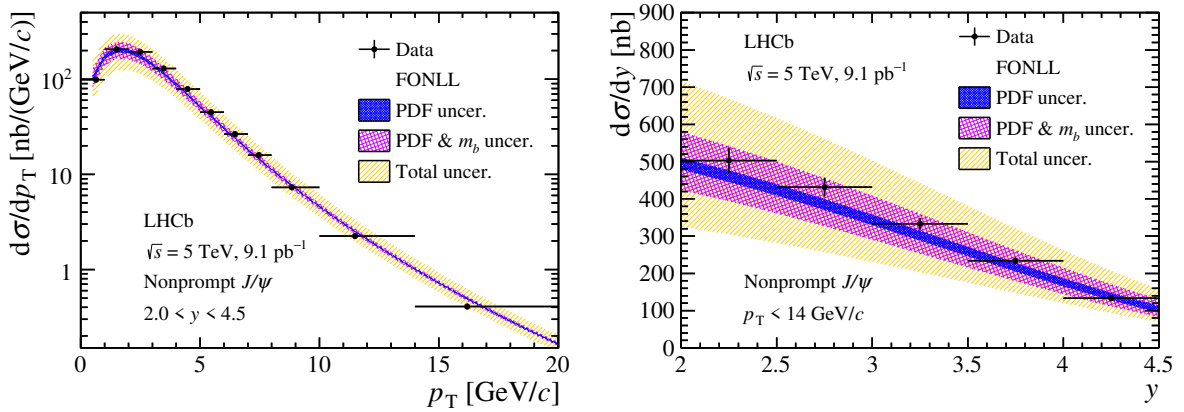

Figure 4: Differential cross-sections (left) $d\sigma/dp_T$ and (right) $d\sigma/dy$ for nonprompt J/ψ mesons compared with FONLL calculations [58, 59]. The orange band shows the total FONLL calculation uncertainty; the violet band shows the uncertainties of PDFs and that due to b-quark mass added in quadrature; the blue band shows only the uncertainties on PDFs.

The production cross-sections of J/ψ mesons at 5 TeV are compared with those previously measured at 8 TeV [13] and 13 TeV [14] in the range $0 < p_T < 14$ GeV/c and $2.0 < y < 4.5$. The ratios of differential cross-sections for prompt J/ψ mesons between 8 TeV and 5 TeV measurements are shown in Fig. 6, and those between 13 TeV and 5 TeV in Fig. 7, both compared with NRQCD and CGC calculations. For nonprompt J/ψ mesons, the ratios of differential cross-sections between 8 TeV and 5 TeV measurements are shown in Fig. 8, and those between 13 TeV and 5 TeV in Fig. 9, compared with FONLL calculations. Some of the systematic uncertainties are considered to fully cancel in the ratio, such as those due to branching fraction and the radiative tail. The uncertainties due to the t_z fit and simulation sample size are taken as uncorrelated between the two measurements, and therefore remain. All other systematic uncertainties are assumed to cancel only partially. For example, the systematic uncertainty due to the luminosity measurement is estimated to be correlated at 50%. The overall uncertainty on the
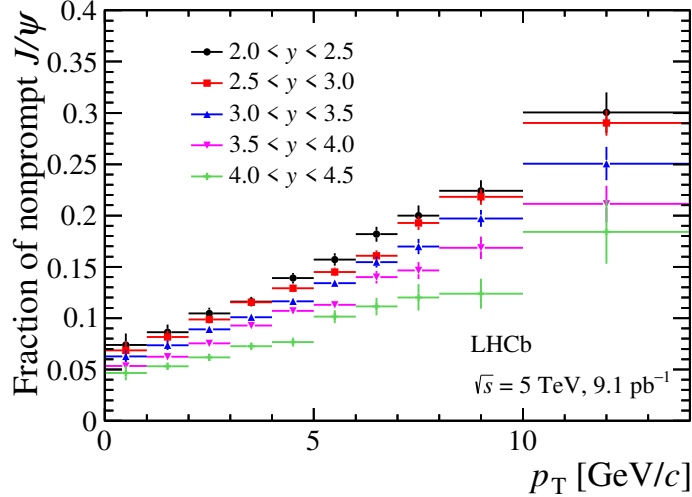
Figure 5: Fraction of nonprompt J/ψ mesons as a function of p_T in intervals of y. The error bars represent the total uncertainties, which are partially correlated between intervals.
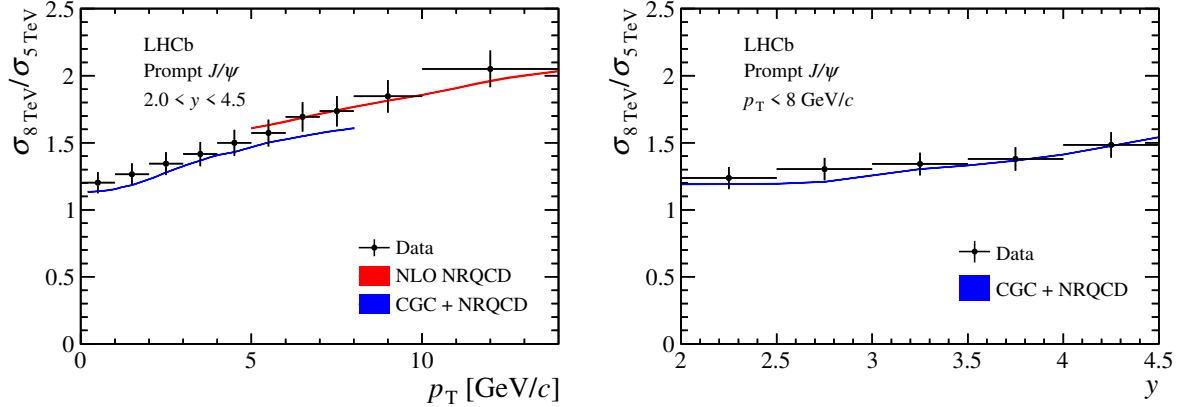

Figure 6: Ratios of differential cross-sections between 8 TeV and 5 TeV measurements as a function of (left) p_T and (right) y for prompt J/ψ mesons compared with NRQCD and CGC calculations [54, 55]. Uncertainties due to the LDMEs determination, renormalisation scales, and factorisation scales are included in the NRQCD and CGC calculations.

measured ratio is dominated by the luminosity measurement for prompt J/ψ mesons, and by the t_z fit and the luminosity measurement for nonprompt J/ψ mesons. For the NRQCD and CGC estimates of the cross-section ratios, the uncertainties due to LDMEs determination, renormalisation scales, and factorisation scales between different energies mostly cancel. For the FONLL calculations, the uncertainty on the ratio is dominated by the uncertainties of PDFs for the low-p_T and large-y regions and by the uncertainty due to the scales of the renormalisation and factorisation for the high-p_T and small-y regions.

Figures 6 and 7 show good agreement between NLO NRQCD calculations and the measurement results in the high-p_T region. The inclusion of CGC effects achieves a reasonable agreement between data and theory in the low-p_T region but a small discrepancy is still observed, which indicates that a pure fixed-order calculation may be insufficient and Sudakov resummation [60] may be required. A comparison of Figs. 6 and 7 suggests that
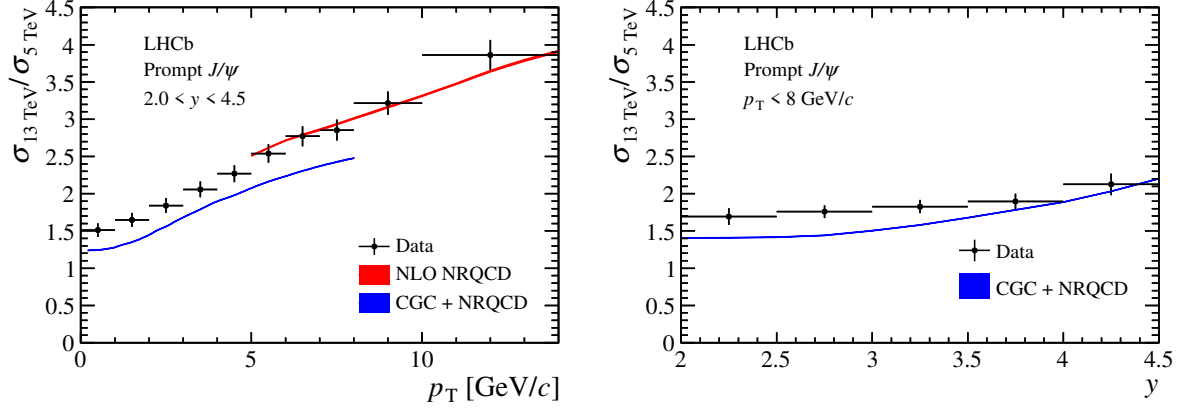
Figure 7: Ratios of differential cross-sections between 13 TeV and 5 TeV measurements as a function of (left) p_T and (right) y for prompt J/ψ mesons compared with NRQCD and CGC calculations [54,55]. Uncertainties due to the LDMEs determination, renormalisation scales, and factorisation scales are included in the NRQCD and CGC calculations.

Figure 8: Ratios of differential cross-sections between 8 TeV and 5 TeV measurements as a function of (left) p_T and (right) y for nonprompt J/ψ mesons compared with FONLL calculations [58,59]. The orange band shows the total FONLL calculation uncertainty; the violet band shows the uncertainties on PDFs and that due to b-quark mass added in quadrature; the red band shows only the uncertainty due to the b-quark mass.

the energy dependence of the cross-sections may differ between the theoretical calculation and the experimental measurements. Figures 8 and 9 show that the FONLL calculations agree with the experimental results for nonprompt J/ψ mesons.

7 Nuclear modification factor

The production cross-sections in pp collisions are essential inputs for the study of nuclear effects in collisions involving heavy ions. Nuclear effects are usually characterized by the nuclear modification factor. In proton-lead (pPb) collisions, this factor, $R_{p\text{Pb}}$, is defined as the production cross-section of a given particle per nucleon pair in pPb collisions divided by that in pp collisions. The previous $R_{p\text{Pb}}$ measurement performed by the LHCb
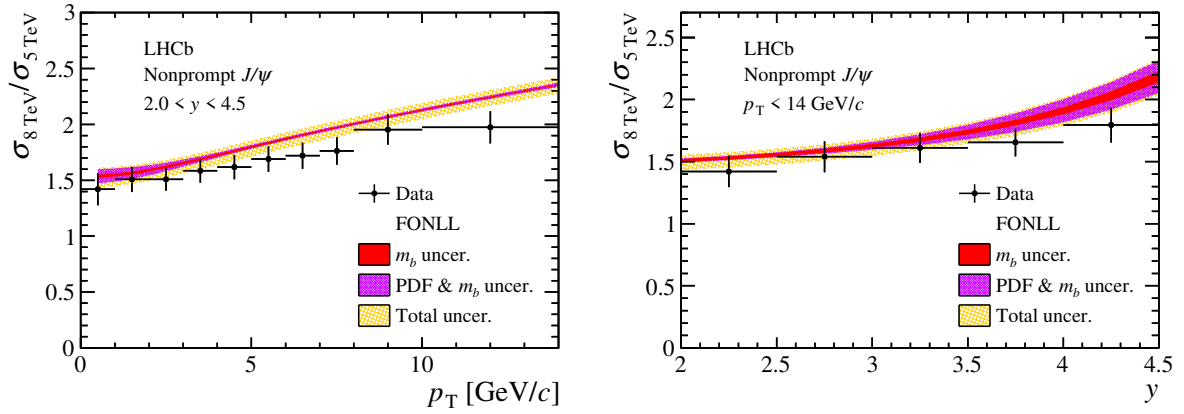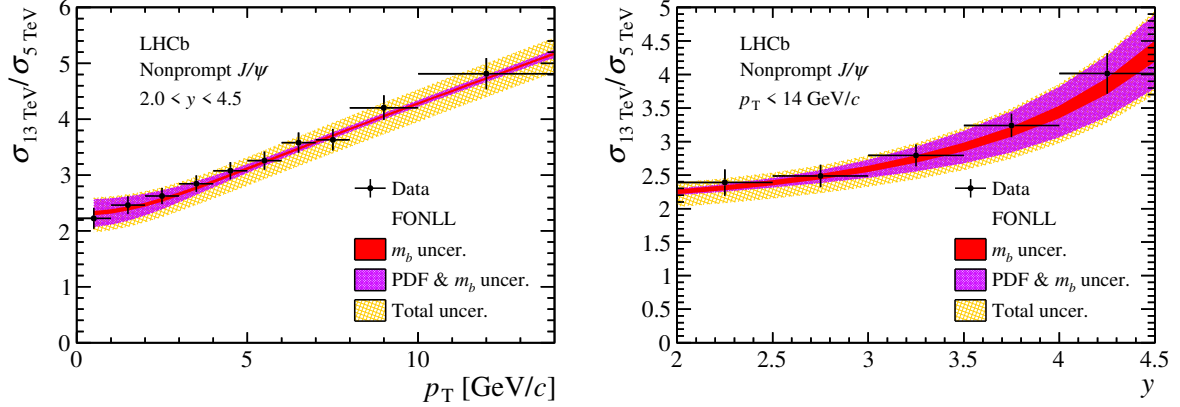
Figure 9: Ratios of differential cross-sections between 13 TeV and 5 TeV measurements as a function of (left) p_{T} and (right) y for nonprompt J/ψ mesons compared with FONLL calculations [58, 59]. The orange band shows the total FONLL calculation uncertainty; the violet band shows the uncertainties on PDFs and that due to b-quark mass added in quadrature; the red band shows only the uncertainty due to b-quark mass.

collaboration at a centre-of-mass energy per nucleon pair of $\sqrt{s_{\mathrm{NN}}} = 5$ TeV [34] made use of J/ψ production cross-sections in pp collisions at 5 TeV derived from an interpolation of LHCb measurements at 2.76, 7 and 8 TeV [11–13] using a power-law fit. Based on the direct measurement presented in this paper, the nuclear modification factor $R_{p\mathrm{Pb}}$ is updated. In the data taking of pPb collisions, two distinct beam configurations are used, pPb and Pbp. In the pPb configuration particles produced in the direction of the proton beam are analysed, while in the Pbp configuration particles are analysed in the Pb beam direction. Rapidity y is defined in the nucleon-nucleon rest frame, and the coverage at LHCb is $1.5 < y < 4.0$ ($-5.0 < y < -2.5$) in the pPb (Pbp) configuration.

The $R_{p\mathrm{Pb}}$ values, as a function of y in the range $p_{\mathrm{T}} < 14$ GeV/c, for prompt and nonprompt J/ψ mesons, are shown in Fig. 10 along with several theoretical predictions. The values are also listed in Table 9 in Appendix A. The predictions are obtained with the nDSg LO nuclear parton distribution function (nPDF) parameterisation [61], the EPS09 LO nPDF parameterisation [61], and the EPS09 NLO nPDF parameterisation [62], and from the fully coherent energy loss (FCEL) model [63]. Conservatively, the systematic uncertainties are assumed to be uncorrelated between the results obtained in pPb and pp collisions. For prompt J/ψ mesons, the measurement agrees with most theoretical calculations, while the calculation with the EPS09 NLO nPDF parameterisation [62] gives a poorer description. The comparison for nonprompt J/ψ mesons shows good agreement.

8   Conclusion

The J/ψ production cross-sections in proton-proton collisions at a centre-of-mass energy $\sqrt{s} = 5$ TeV are studied using a data sample corresponding to an integrated luminosity of 9.18 ± 0.35 pb^{-1} collected by the LHCb detector. The J/ψ differential cross-sections, as a function of p_{T} and y, are measured separately for prompt and nonprompt J/ψ mesons in the range $0 < p_{\mathrm{T}} < 20$ GeV/c and $2.0 < y < 4.5$. The J/ψ production cross-section ratios between 8 TeV and 5 TeV, and between 13 TeV and 5 TeV are also determined and
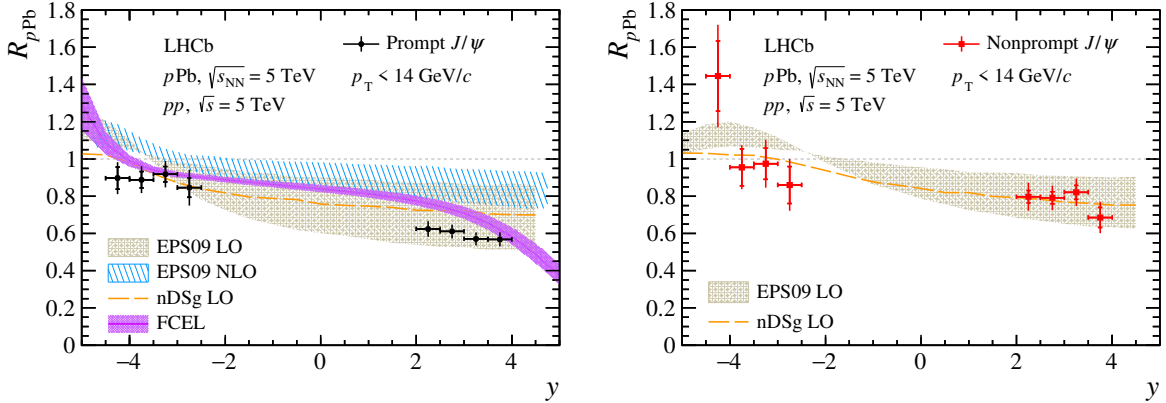
Figure 10: Nuclear modification factor $R_{p\mathrm{Pb}}$ as a function of y for (left) prompt and (right) nonprompt J/ψ mesons, together with the theoretical predictions from (yellow dashed line and brown band) Ref. [61], (blue band) Ref. [62], and (violet solid line with band) Ref. [63,64]. In the data points the full error bars represent the statistical and systematic uncertainties added in quadrature, while the smaller ones represent the statistical uncertainties.

compared with the theory models. The measured prompt J/ψ results are in good agreement with NLO NRQCD calculations in the high-p_{T} region. A small tension is observed between data for prompt J/ψ in the low-p_{T} region and NRQCD and CGC calculations, which may indicate the need for further corrections in the theory model. The FONLL calculations describe the measured results for nonprompt J/ψ mesons well. The nuclear modification factor in proton-lead collisions for J/ψ mesons at a centre-of-mass energy per nucleon pair of $\sqrt{s_{\mathrm{NN}}} = 5\,\mathrm{TeV}$ is updated and supersedes that in the previous publication [34].

Acknowledgements

Appendices

A Result tables

Table 2: Double-differential production cross-sections $\frac{\mathrm{d}^2\sigma}{\mathrm{d}p_\mathrm{T}\mathrm{d}y}$[nb/(GeV/$c$) per unit rapidity] for prompt J/ψ mesons in (p_T,y) intervals. The first uncertainties are statistical, the second are correlated systematic uncertainties shared between intervals, the third are uncorrelated systematic uncertainties, and the last are correlated between p_T intervals and uncorrelated between y intervals.

p_T [GeV/c]	$2.0 < y < 2.5$	$2.5 < y < 3.0$
$0-1$	$686.03 \pm 6.80 \pm 35.11 \pm 9.03 \pm 4.92$	$640.03 \pm 3.70 \pm 22.97 \pm 2.78 \pm 5.06$
$1-2$	$1253.23 \pm 8.66 \pm 55.59 \pm 15.31 \pm 9.82$	$1173.73 \pm 4.95 \pm 39.14 \pm 4.68 \pm 7.58$
$2-3$	$964.82 \pm 6.79 \pm 40.41 \pm 12.19 \pm 5.23$	$917.24 \pm 4.09 \pm 30.11 \pm 2.86 \pm 3.76$
$3-4$	$575.26 \pm 4.74 \pm 21.54 \pm 7.51 \pm 2.89$	$540.97 \pm 2.82 \pm 17.21 \pm 2.52 \pm 1.80$
$4-5$	$305.38 \pm 2.89 \pm 10.65 \pm 2.93 \pm 1.28$	$286.82 \pm 1.76 \pm 8.98 \pm 1.74 \pm 1.10$
$5-6$	$159.48 \pm 1.84 \pm 5.44 \pm 1.51 \pm 0.72$	$143.21 \pm 1.12 \pm 4.46 \pm 1.11 \pm 0.49$
$6-7$	$79.23 \pm 1.19 \pm 2.63 \pm 1.02 \pm 0.26$	$73.00 \pm 0.75 \pm 2.26 \pm 0.66 \pm 0.25$
$7-8$	$43.60 \pm 0.82 \pm 1.43 \pm 0.77 \pm 0.01$	$36.67 \pm 0.52 \pm 1.13 \pm 0.32 \pm 0.00$
$8-10$	$18.11 \pm 0.34 \pm 0.59 \pm 0.24 \pm 0.08$	$15.17 \pm 0.23 \pm 0.47 \pm 0.15 \pm 0.04$
$10-14$	$4.15 \pm 0.11 \pm 0.13 \pm 0.07 \pm 0.02$	$3.34 \pm 0.07 \pm 0.11 \pm 0.04 \pm 0.01$
p_T [GeV/c]	$3.0 < y < 3.5$	$3.5 < y < 4.0$
$0-1$	$589.31 \pm 3.22 \pm 19.72 \pm 1.82 \pm 2.99$	$515.07 \pm 2.78 \pm 17.29 \pm 1.72 \pm 0.30$
$1-2$	$1056.67 \pm 4.29 \pm 34.89 \pm 4.63 \pm 4.82$	$911.86 \pm 3.68 \pm 30.29 \pm 2.93 \pm 0.63$
$2-3$	$804.99 \pm 3.45 \pm 26.10 \pm 6.15 \pm 1.60$	$681.00 \pm 3.04 \pm 22.56 \pm 1.99 \pm 1.78$
$3-4$	$461.97 \pm 2.24 \pm 14.45 \pm 1.89 \pm 0.81$	$370.70 \pm 2.08 \pm 11.71 \pm 1.36 \pm 0.55$
$4-5$	$236.68 \pm 1.47 \pm 7.28 \pm 0.94 \pm 0.29$	$185.30 \pm 1.36 \pm 5.81 \pm 1.72 \pm 0.32$
$5-6$	$115.63 \pm 0.95 \pm 3.55 \pm 1.17 \pm 0.17$	$86.71 \pm 0.86 \pm 2.75 \pm 0.78 \pm 0.01$
$6-7$	$56.50 \pm 0.64 \pm 1.73 \pm 0.42 \pm 0.03$	$41.09 \pm 0.57 \pm 1.34 \pm 0.38 \pm 0.10$
$7-8$	$28.48 \pm 0.44 \pm 0.87 \pm 0.28 \pm 0.10$	$20.85 \pm 0.39 \pm 0.71 \pm 0.28 \pm 0.03$
$8-10$	$11.35 \pm 0.19 \pm 0.35 \pm 0.11 \pm 0.03$	$7.59 \pm 0.16 \pm 0.27 \pm 0.11 \pm 0.01$
$10-14$	$2.26 \pm 0.06 \pm 0.08 \pm 0.04 \pm 0.00$	$1.38 \pm 0.05 \pm 0.05 \pm 0.03 \pm 0.01$
p_T [GeV/c]	$4.0 < y < 4.5$	
$0-1$	$452.31 \pm 3.21 \pm 17.49 \pm 2.85 \pm 2.79$	
$1-2$	$731.38 \pm 4.04 \pm 27.48 \pm 3.52 \pm 0.74$	
$2-3$	$485.71 \pm 3.25 \pm 19.15 \pm 3.16 \pm 0.50$	
$3-4$	$240.13 \pm 2.17 \pm 9.05 \pm 2.68 \pm 0.21$	
$4-5$	$108.46 \pm 1.33 \pm 4.16 \pm 1.18 \pm 0.25$	
$5-6$	$49.12 \pm 0.84 \pm 1.90 \pm 0.59 \pm 0.08$	
$6-7$	$22.06 \pm 0.52 \pm 0.86 \pm 0.35 \pm 0.02$	
$7-8$	$10.36 \pm 0.34 \pm 0.40 \pm 0.24 \pm 0.03$	
$8-10$	$3.82 \pm 0.14 \pm 0.15 \pm 0.09 \pm 0.01$	
$10-14$	$0.58 \pm 0.04 \pm 0.02 \pm 0.02 \pm 0.00$	

Table 3: Double-differential production cross-sections $\frac{\mathrm{d}^2\sigma}{\mathrm{d}p_{\mathrm{T}}\mathrm{d}y}$[nb/(GeV/$c$) per unit rapidity] for nonprompt J/ψ mesons in (p_{T},y) intervals. The first uncertainties are statistical, the second are correlated systematic uncertainties shared between intervals, the third are uncorrelated systematic uncertainties, and the last are correlated between p_{T} intervals and uncorrelated between y intervals

p_{T} [GeV/c]	$2.0 < y < 2.5$	$2.5 < y < 3.0$
$0-1$	$56.02 \pm 1.88 \pm 2.87 \pm 1.35 \pm 7.96$	$47.72 \pm 1.00 \pm 1.71 \pm 0.48 \pm 5.71$
$1-2$	$120.67 \pm 2.48 \pm 5.35 \pm 1.88 \pm 9.89$	$105.37 \pm 1.37 \pm 3.51 \pm 2.07 \pm 7.81$
$2-3$	$117.89 \pm 2.23 \pm 4.94 \pm 2.46 \pm 5.15$	$101.93 \pm 1.26 \pm 3.35 \pm 1.12 \pm 3.66$
$3-4$	$78.32 \pm 1.67 \pm 2.93 \pm 1.36 \pm 2.57$	$71.20 \pm 0.97 \pm 2.27 \pm 0.52 \pm 1.68$
$4-5$	$51.65 \pm 1.24 \pm 1.80 \pm 0.89 \pm 1.18$	$42.83 \pm 0.69 \pm 1.34 \pm 0.41 \pm 0.99$
$5-6$	$30.55 \pm 0.84 \pm 1.04 \pm 0.51 \pm 0.64$	$24.58 \pm 0.48 \pm 0.77 \pm 0.30 \pm 0.43$
$6-7$	$18.43 \pm 0.60 \pm 0.61 \pm 0.39 \pm 0.22$	$14.39 \pm 0.36 \pm 0.45 \pm 0.22 \pm 0.22$
$7-8$	$11.57 \pm 0.45 \pm 0.38 \pm 0.36 \pm 0.01$	$9.13 \pm 0.27 \pm 0.28 \pm 0.13 \pm 0.00$
$8-10$	$5.29 \pm 0.19 \pm 0.17 \pm 0.12 \pm 0.07$	$4.31 \pm 0.13 \pm 0.13 \pm 0.06 \pm 0.03$
$10-14$	$1.80 \pm 0.07 \pm 0.06 \pm 0.08 \pm 0.02$	$1.39 \pm 0.05 \pm 0.04 \pm 0.02 \pm 0.01$

p_{T} [GeV/c]	$3.0 < y < 3.5$	$3.5 < y < 4.0$
$0-1$	$40.73 \pm 0.84 \pm 1.36 \pm 0.38 \pm 3.55$	$30.25 \pm 0.76 \pm 1.02 \pm 0.40 \pm 0.34$
$1-2$	$85.36 \pm 1.15 \pm 2.82 \pm 1.56 \pm 5.16$	$61.11 \pm 1.00 \pm 2.03 \pm 0.60 \pm 0.64$
$2-3$	$79.84 \pm 1.00 \pm 2.59 \pm 1.19 \pm 1.59$	$55.94 \pm 0.89 \pm 1.85 \pm 0.79 \pm 1.80$
$3-4$	$51.96 \pm 0.75 \pm 1.62 \pm 0.49 \pm 0.75$	$38.20 \pm 0.69 \pm 1.21 \pm 0.42 \pm 0.59$
$4-5$	$31.75 \pm 0.55 \pm 0.98 \pm 0.27 \pm 0.28$	$22.43 \pm 0.49 \pm 0.70 \pm 0.31 \pm 0.36$
$5-6$	$18.22 \pm 0.40 \pm 0.56 \pm 0.26 \pm 0.17$	$10.97 \pm 0.33 \pm 0.35 \pm 0.16 \pm 0.01$
$6-7$	$10.36 \pm 0.29 \pm 0.32 \pm 0.20 \pm 0.03$	$6.83 \pm 0.25 \pm 0.22 \pm 0.12 \pm 0.11$
$7-8$	$6.00 \pm 0.22 \pm 0.18 \pm 0.09 \pm 0.10$	$3.60 \pm 0.17 \pm 0.12 \pm 0.10 \pm 0.03$
$8-10$	$2.87 \pm 0.10 \pm 0.09 \pm 0.04 \pm 0.02$	$1.57 \pm 0.08 \pm 0.06 \pm 0.06 \pm 0.01$
$10-14$	$0.77 \pm 0.04 \pm 0.03 \pm 0.03 \pm 0.00$	$0.39 \pm 0.03 \pm 0.01 \pm 0.01 \pm 0.01$

p_{T} [GeV/c]	$4.0 < y < 4.5$
$0-1$	$22.40 \pm 0.90 \pm 0.87 \pm 0.45 \pm 3.29$
$1-2$	$40.68 \pm 1.11 \pm 1.53 \pm 0.61 \pm 0.82$
$2-3$	$31.22 \pm 0.91 \pm 1.23 \pm 0.71 \pm 0.52$
$3-4$	$18.68 \pm 0.66 \pm 0.70 \pm 0.44 \pm 0.22$
$4-5$	$9.00 \pm 0.42 \pm 0.34 \pm 0.18 \pm 0.26$
$5-6$	$5.51 \pm 0.30 \pm 0.21 \pm 0.14 \pm 0.10$
$6-7$	$2.84 \pm 0.20 \pm 0.11 \pm 0.09 \pm 0.02$
$7-8$	$1.44 \pm 0.13 \pm 0.06 \pm 0.07 \pm 0.04$
$8-10$	$0.53 \pm 0.06 \pm 0.02 \pm 0.02 \pm 0.01$
$10-14$	$0.15 \pm 0.02 \pm 0.01 \pm 0.01 \pm 0.01$

Table 4: Single-differential production cross-sections $\frac{\mathrm{d}\sigma}{\mathrm{d}p_\mathrm{T}}$ [nb/(GeV/c)] for prompt J/ψ mesons in the rapidity range $2-4.5$. The first uncertainties are statistical, the second are correlated systematic uncertainties shared between intervals, and the last are uncorrelated systematic uncertainties.

p_T [GeV/c]	$2.0 < y < 4.5$
$0-1$	$1441.38 \pm 4.70 \pm 53.61 \pm 5.09$
$1-2$	$2563.43 \pm 6.08 \pm 90.61 \pm 8.64$
$2-3$	$1926.88 \pm 4.86 \pm 67.32 \pm 7.22$
$3-4$	$1094.51 \pm 3.34 \pm 36.15 \pm 4.34$
$4-5$	$561.32 \pm 2.08 \pm 18.10 \pm 2.05$
$5-6$	$277.07 \pm 1.32 \pm\ \ 8.89 \pm 1.21$
$6-7$	$135.95 \pm 0.86 \pm\ \ 4.34 \pm 0.69$
$7-8$	$69.98 \pm 0.59 \pm\ \ 2.23 \pm 0.48$
$8-10$	$28.02 \pm 0.25 \pm\ \ 0.90 \pm 0.17$
$10-14$	$5.85 \pm 0.08 \pm\ \ 0.19 \pm 0.05$
$14-20$	$0.66 \pm 0.02 \pm\ \ 0.02 \pm 0.02$

Table 5: Single-differential production cross-sections $\frac{\mathrm{d}\sigma}{\mathrm{d}p_\mathrm{T}}$ [nb/(GeV/c)] for nonprompt J/ψ mesons in the rapidity range $2-4.5$. The first uncertainties are statistical, the second are correlated systematic uncertainties shared between intervals, and the last are uncorrelated systematic uncertainties.

p_T [GeV/c]	$2.0 < y < 4.5$
$0-1$	$98.56 \pm 1.29 \pm\ \ 6.61 \pm 0.80$
$1-2$	$206.60 \pm 1.70 \pm 10.03 \pm 1.65$
$2-3$	$193.41 \pm 1.51 \pm\ \ 7.58 \pm 1.57$
$3-4$	$129.17 \pm 1.14 \pm\ \ 4.56 \pm 0.83$
$4-5$	$78.83 \pm 0.83 \pm\ \ 2.66 \pm 0.54$
$5-6$	$44.91 \pm 0.57 \pm\ \ 1.49 \pm 0.34$
$6-7$	$26.43 \pm 0.41 \pm\ \ 0.86 \pm 0.25$
$7-8$	$15.88 \pm 0.31 \pm\ \ 0.51 \pm 0.20$
$8-10$	$7.29 \pm 0.14 \pm\ \ 0.24 \pm 0.08$
$10-14$	$2.24 \pm 0.05 \pm\ \ 0.07 \pm 0.05$
$14-20$	$0.41 \pm 0.02 \pm\ \ 0.01 \pm 0.01$

Table 6: Single-differential production cross-sections $\frac{\mathrm{d}\sigma}{\mathrm{d}y}$ [nb per unit rapidity] for prompt J/ψ mesons. The first uncertainties are statistical, the second are correlated systematic uncertainties shared between intervals, and the last are uncorrelated systematic uncertainties.

y	$0 < p_\mathrm{T} < 14\,\mathrm{GeV}/c$	$0 < p_\mathrm{T} < 8\,\mathrm{GeV}/c$
$2.0-2.5$	$4119.9 \pm 14.3 \pm 170.6 \pm 34.3$	$4067.0 \pm 14.3 \pm 169.1 \pm 34.1$
$2.5-3.0$	$3855.4 \pm\ \ 8.3 \pm 126.8 \pm 21.3$	$3811.7 \pm\ \ 8.2 \pm 125.4 \pm 21.2$
$3.0-3.5$	$3382.0 \pm\ \ 7.0 \pm 109.1 \pm 13.7$	$3350.2 \pm\ \ 7.0 \pm 108.1 \pm 13.6$
$3.5-4.0$	$2833.3 \pm\ \ 6.2 \pm\ \ 92.6 \pm\ \ 5.9$	$2812.6 \pm\ \ 6.2 \pm\ \ 91.8 \pm\ \ 5.9$
$4.0-4.5$	$2109.5 \pm\ \ 6.7 \pm\ \ 80.0 \pm\ \ 7.8$	$2099.5 \pm\ \ 6.7 \pm\ \ 79.6 \pm\ \ 7.8$

Table 7: Single-differential production cross-sections $\frac{d\sigma}{dy}$[nb per unit rapidity] for nonprompt J/ψ mesons. The first uncertainties are statistical, the second are correlated systematic uncertainties shared between intervals, and the last are uncorrelated systematic uncertainties.

y	$0 < p_{\mathrm{T}} < 14\,\mathrm{GeV}/c$
$2.0 - 2.5$	$502.9 \pm 4.5 \pm 20.0 \pm 28.1$
$2.5 - 3.0$	$431.3 \pm 2.5 \pm 14.0 \pm 20.8$
$3.0 - 3.5$	$333.0 \pm 2.1 \pm 10.7 \pm 11.9$
$3.5 - 4.0$	$234.0 \pm 1.8 \pm\ \ 7.6 \pm\ \ 4.1$
$4.0 - 4.5$	$133.4 \pm 1.9 \pm\ \ 5.1 \pm\ \ 5.4$

Table 8: Fraction of nonprompt J/ψ mesons (in %) in (p_{T},y) intervals. The first uncertainty is statistical and the second is systematic.

$p_{\mathrm{T}}\ [\mathrm{GeV}/c\,]$	$2.0 < y < 2.5$	$2.5 < y < 3.0$	$3.0 < y < 3.5$
$0 - 1$	$7.4 \pm 0.3 \pm 1.1$	$6.8 \pm 0.1 \pm 0.8$	$6.3 \pm 0.1 \pm 0.6$
$1 - 2$	$8.6 \pm 0.2 \pm 0.7$	$8.2 \pm 0.1 \pm 0.6$	$7.4 \pm 0.1 \pm 0.5$
$2 - 3$	$10.5 \pm 0.2 \pm 0.5$	$9.9 \pm 0.1 \pm 0.4$	$8.9 \pm 0.1 \pm 0.2$
$3 - 4$	$11.6 \pm 0.3 \pm 0.4$	$11.5 \pm 0.2 \pm 0.3$	$10.1 \pm 0.2 \pm 0.2$
$4 - 5$	$13.9 \pm 0.4 \pm 0.4$	$12.9 \pm 0.2 \pm 0.3$	$11.6 \pm 0.2 \pm 0.1$
$5 - 6$	$15.7 \pm 0.5 \pm 0.4$	$14.5 \pm 0.3 \pm 0.3$	$13.4 \pm 0.3 \pm 0.2$
$6 - 7$	$18.2 \pm 0.6 \pm 0.4$	$16.1 \pm 0.4 \pm 0.3$	$15.5 \pm 0.5 \pm 0.3$
$7 - 8$	$20.0 \pm 0.8 \pm 0.6$	$19.3 \pm 0.6 \pm 0.2$	$17.0 \pm 0.7 \pm 0.3$
$8 - 10$	$22.4 \pm 0.9 \pm 0.5$	$21.8 \pm 0.7 \pm 0.3$	$19.7 \pm 0.8 \pm 0.3$
$10 - 14$	$30.0 \pm 1.4 \pm 1.4$	$29.0 \pm 1.2 \pm 0.5$	$25.1 \pm 1.3 \pm 0.9$
$p_{\mathrm{T}}\ [\mathrm{GeV}/c\,]$	$3.5 < y < 4$	$4 < y < 4.5$	
$0 - 1$	$5.3 \pm 0.1 \pm 0.1$	$4.6 \pm 0.2 \pm 0.7$	
$1 - 2$	$6.2 \pm 0.1 \pm 0.1$	$5.3 \pm 0.1 \pm 0.1$	
$2 - 3$	$7.5 \pm 0.1 \pm 0.3$	$6.2 \pm 0.2 \pm 0.2$	
$3 - 4$	$9.3 \pm 0.2 \pm 0.2$	$7.3 \pm 0.3 \pm 0.2$	
$4 - 5$	$10.7 \pm 0.2 \pm 0.2$	$7.7 \pm 0.4 \pm 0.2$	
$5 - 6$	$11.3 \pm 0.4 \pm 0.1$	$10.2 \pm 0.6 \pm 0.2$	
$6 - 7$	$14.0 \pm 0.5 \pm 0.3$	$11.1 \pm 0.8 \pm 0.2$	
$7 - 8$	$14.6 \pm 0.8 \pm 0.3$	$12.0 \pm 1.2 \pm 0.5$	
$8 - 10$	$16.9 \pm 0.9 \pm 0.6$	$12.4 \pm 1.4 \pm 0.5$	
$10 - 14$	$21.1 \pm 1.7 \pm 0.7$	$18.4 \pm 2.8 \pm 1.4$	

Table 9: Nuclear modification factor $R_{p\mathrm{Pb}}$ as a function of y with $p_\mathrm{T} < 14\,\mathrm{GeV}/c$. The first uncertainty is statistical and the second is systematic.

y	prompt J/ψ	nonprompt J/ψ
$(-4.5, -4.0)$	$0.897 \pm 0.060 \pm 0.061$	$1.445 \pm 0.189 \pm 0.201$
$(-4.0, -3.5)$	$0.888 \pm 0.044 \pm 0.056$	$0.955 \pm 0.099 \pm 0.064$
$(-3.5, -3.0)$	$0.918 \pm 0.041 \pm 0.058$	$0.974 \pm 0.084 \pm 0.097$
$(-3.0, -2.5)$	$0.846 \pm 0.052 \pm 0.082$	$0.860 \pm 0.099 \pm 0.097$
$(\ 2.0, \ \ 2.5)$	$0.624 \pm 0.014 \pm 0.039$	$0.797 \pm 0.033 \pm 0.068$
$(\ 2.5, \ \ 3.0)$	$0.611 \pm 0.012 \pm 0.035$	$0.791 \pm 0.032 \pm 0.058$
$(\ 3.0, \ \ 3.5)$	$0.571 \pm 0.012 \pm 0.033$	$0.821 \pm 0.038 \pm 0.064$
$(\ 3.5, \ \ 4.0)$	$0.568 \pm 0.015 \pm 0.035$	$0.686 \pm 0.054 \pm 0.065$

Table 10: Cross-section ratios between 8 TeV and 5 TeV measurements for prompt J/ψ mesons as a function of p_T with $2.0 < y < 4.5$. The first uncertainty is statistical and the second is systematic.

$p_\mathrm{T}\ [\,\mathrm{GeV}/c\,]$	$2.0 < y < 4.5$
$0 - 1$	$1.20 \pm 0.01 \pm 0.08$
$1 - 2$	$1.27 \pm 0.01 \pm 0.08$
$2 - 3$	$1.34 \pm 0.01 \pm 0.09$
$3 - 4$	$1.42 \pm 0.01 \pm 0.09$
$4 - 5$	$1.50 \pm 0.01 \pm 0.10$
$5 - 6$	$1.57 \pm 0.01 \pm 0.10$
$6 - 7$	$1.69 \pm 0.01 \pm 0.11$
$7 - 8$	$1.74 \pm 0.02 \pm 0.11$
$8 - 10$	$1.85 \pm 0.02 \pm 0.12$
$10 - 14$	$2.05 \pm 0.03 \pm 0.13$

Table 11: Cross-section ratios between 8 TeV and 5 TeV measurements for prompt J/ψ mesons as a function of y with $p_\mathrm{T} < 8\,\mathrm{GeV}/c$. The first uncertainty is statistical and the second is systematic.

y	$0 < p_\mathrm{T} < 8\,\mathrm{GeV}/c$
$2.0 - 2.5$	$1.24 \pm 0.01 \pm 0.08$
$2.5 - 3.0$	$1.30 \pm 0.00 \pm 0.08$
$3.0 - 3.5$	$1.34 \pm 0.00 \pm 0.09$
$3.5 - 4.0$	$1.38 \pm 0.00 \pm 0.09$
$4.0 - 4.5$	$1.48 \pm 0.01 \pm 0.10$

Table 12: Cross-section ratios between 13 TeV and 5 TeV measurements for prompt J/ψ mesons as a function of p_{T} with $2.0 < y < 4.5$. The first uncertainty is statistical and the second is systematic.

$p_{\mathrm{T}}\,[\,\mathrm{GeV}/c\,]$	$2.0 < y < 4.5$
$0 - 1$	$1.51 \pm 0.01 \pm 0.08$
$1 - 2$	$1.65 \pm 0.01 \pm 0.09$
$2 - 3$	$1.84 \pm 0.01 \pm 0.09$
$3 - 4$	$2.06 \pm 0.01 \pm 0.10$
$4 - 5$	$2.27 \pm 0.01 \pm 0.11$
$5 - 6$	$2.54 \pm 0.02 \pm 0.12$
$6 - 7$	$2.77 \pm 0.03 \pm 0.13$
$7 - 8$	$2.85 \pm 0.03 \pm 0.13$
$8 - 10$	$3.22 \pm 0.04 \pm 0.15$
$10 - 14$	$3.86 \pm 0.07 \pm 0.18$

Table 13: Cross-section ratios between 13 TeV and 5 TeV measurements for prompt J/ψ mesons as a function of y with $p_{\mathrm{T}} < 8\,\mathrm{GeV}/c$. The first uncertainty is statistical and the second is systematic.

y	$0 < p_{\mathrm{T}} < 8\,\mathrm{GeV}/c$
$2.0 - 2.5$	$1.70 \pm 0.01 \pm 0.10$
$2.5 - 3.0$	$1.76 \pm 0.01 \pm 0.08$
$3.0 - 3.5$	$1.83 \pm 0.01 \pm 0.08$
$3.5 - 4.0$	$1.90 \pm 0.01 \pm 0.10$
$4.0 - 4.5$	$2.13 \pm 0.01 \pm 0.13$

Table 14: Cross-section ratios between 8 TeV and 5 TeV measurements for nonprompt J/ψ mesons as a function of p_{T} with $2.0 < y < 4.5$. The first uncertainty is statistical and the second is systematic.

$p_{\mathrm{T}}\,[\,\mathrm{GeV}/c\,]$	$2.0 < y < 4.5$
$0 - 1$	$1.42 \pm 0.03 \pm 0.14$
$1 - 2$	$1.51 \pm 0.02 \pm 0.11$
$2 - 3$	$1.51 \pm 0.02 \pm 0.10$
$3 - 4$	$1.59 \pm 0.02 \pm 0.10$
$4 - 5$	$1.62 \pm 0.02 \pm 0.11$
$5 - 6$	$1.69 \pm 0.03 \pm 0.11$
$6 - 7$	$1.72 \pm 0.03 \pm 0.11$
$7 - 8$	$1.76 \pm 0.04 \pm 0.12$
$8 - 10$	$1.95 \pm 0.04 \pm 0.13$
$10 - 14$	$1.97 \pm 0.05 \pm 0.13$

Table 15: Cross-section ratios between 8 TeV and 5 TeV measurements for nonprompt J/ψ mesons as a function of y with $p_{\mathrm{T}} < 14\,\mathrm{GeV}/c$. The first uncertainty is statistical and the second is systematic.

y	$0 < p_{\mathrm{T}} < 14\,\mathrm{GeV}/c$
$2.0 - 2.5$	$1.42 \pm 0.02 \pm 0.12$
$2.5 - 3.0$	$1.54 \pm 0.01 \pm 0.13$
$3.0 - 3.5$	$1.61 \pm 0.01 \pm 0.12$
$3.5 - 4.0$	$1.65 \pm 0.02 \pm 0.11$
$4.0 - 4.5$	$1.80 \pm 0.03 \pm 0.14$

Table 16: Cross-section ratios between 13 TeV and 5 TeV measurements for nonprompt J/ψ mesons as a function of p_{T} with $2.0 < y < 4.5$. The first uncertainty is statistical and the second is systematic.

$p_{\mathrm{T}}\,[\,\mathrm{GeV}/c\,]$	$2.0 < y < 4.5$
$0 - 1$	$2.23 \pm 0.05 \pm 0.17$
$1 - 2$	$2.46 \pm 0.03 \pm 0.16$
$2 - 3$	$2.62 \pm 0.03 \pm 0.14$
$3 - 4$	$2.85 \pm 0.04 \pm 0.14$
$4 - 5$	$3.08 \pm 0.05 \pm 0.15$
$5 - 6$	$3.26 \pm 0.06 \pm 0.15$
$6 - 7$	$3.58 \pm 0.07 \pm 0.17$
$7 - 8$	$3.63 \pm 0.09 \pm 0.17$
$8 - 10$	$4.21 \pm 0.10 \pm 0.20$
$10 - 14$	$4.81 \pm 0.14 \pm 0.24$

Table 17: Cross-section ratios between 13 TeV and 5 TeV measurements for nonprompt J/ψ mesons as a function of y with $p_{\mathrm{T}} < 14\,\mathrm{GeV}/c$. The first uncertainty is statistical and the second is systematic.

y	$0 < p_{\mathrm{T}} < 14\,\mathrm{GeV}/c$
$2.0 - 2.5$	$2.39 \pm 0.03 \pm 0.19$
$2.5 - 3.0$	$2.49 \pm 0.02 \pm 0.17$
$3.0 - 3.5$	$2.79 \pm 0.03 \pm 0.16$
$3.5 - 4.0$	$3.24 \pm 0.04 \pm 0.17$
$4.0 - 4.5$	$4.02 \pm 0.08 \pm 0.29$

B Dependence of cross-sections on the polarisation

The angular distribution of the $J/\psi \to \mu^+ \mu^-$ decay is described by

$$\frac{\mathrm{d}^2 N}{\mathrm{d}\cos\theta\mathrm{d}\phi} \propto 1 + \lambda_\theta \cos^2\theta + \lambda_{\theta\phi} \sin 2\theta \cos\phi + \lambda_\phi \sin^2\theta \cos 2\phi, \tag{3}$$

where θ and ϕ are the polar and azimuthal angles between the direction of μ^+ and the chosen polarisation axis, and λ_θ, $\lambda_{\theta\phi}$ and λ_ϕ are polarisation parameters. In the helicity frame, the polarisation axis coincides with the flight direction of the J/ψ meson in the centre-of-mass frame of the colliding hadrons. The detection efficiency of the J/ψ mesons is function of the polarisation, especially of λ_θ. Zero polarisation is assumed in the simulation since there is no prior knowledge of the polarisation of the J/ψ mesons in pp collisions at $5\,\mathrm{TeV}$, and only small longitudinal polarisations have been found in the J/ψ polarisation analyses at the LHC [53, 65, 66].

To evaluate the change of results assuming a non-zero polarisation, we reweight the angular distribution of the muon tracks in rest frame of the J/ψ mesons in simulation and calculate the change in the total efficiency, which impacts the cross-sections. The relative change of the cross-section for a polarisation of $\lambda_\theta = -0.2$ [53] in the helicity frame compared to zero polarisation in each (p_T, y) interval is given in Table 18. In addition, the relative change of the cross-section for a polarisation of $\lambda_\theta = -1$ $(+1)$ in the helicity frame, which corresponds to the fully longitudinally (transversely) polarised scenario, compared to zero polarisation in each (p_T, y) interval is given in Table 19 (20).

Table 18: Relative changes of cross-sections (in %), for a polarisation of $\lambda_\theta = -0.2$ rather than zero, in (p_T, y) intervals.

p_T [GeV/c]	$2.0 < y < 2.5$	$2.5 < y < 3.0$	$3.0 < y < 3.5$	$3.5 < y < 4.0$	$4.0 < y < 4.5$
$0-1$	-5.91 ± 0.83	-4.47 ± 0.42	-2.94 ± 0.37	-2.39 ± 0.43	-1.95 ± 0.77
$1-2$	-5.22 ± 0.59	-4.05 ± 0.32	-2.47 ± 0.29	-1.38 ± 0.35	-0.47 ± 0.60
$2-3$	-4.38 ± 0.63	-3.21 ± 0.36	-1.62 ± 0.33	-0.49 ± 0.41	0.55 ± 0.72
$3-4$	-4.20 ± 0.75	-3.09 ± 0.42	-1.60 ± 0.40	-0.30 ± 0.51	0.56 ± 0.93
$4-5$	-4.14 ± 0.90	-3.15 ± 0.50	-1.80 ± 0.49	-0.83 ± 0.63	0.47 ± 1.16
$5-6$	-4.00 ± 1.06	-3.00 ± 0.61	-1.87 ± 0.62	-1.10 ± 0.80	0.19 ± 1.52
$6-7$	-3.77 ± 1.30	-2.81 ± 0.76	-1.89 ± 0.79	-1.45 ± 1.05	-0.41 ± 1.96
$7-8$	-3.63 ± 1.61	-2.70 ± 0.96	-1.76 ± 1.04	-1.63 ± 1.37	-0.55 ± 2.66
$8-10$	-3.23 ± 1.52	-2.32 ± 0.96	-1.68 ± 1.08	-1.78 ± 1.50	-1.02 ± 2.92
$10-14$	-2.85 ± 1.88	-2.04 ± 1.28	-1.47 ± 1.54	-1.44 ± 2.22	-1.29 ± 5.07
$14-20$	-1.55 ± 1.87 $(2.0 < y < 4.5)$				

Table 19: Relative change of cross-sections (in %), for a polarisation of $\lambda_\theta = -1$ rather than zero, in (p_{T},y) intervals.

p_{T} [GeV/c]	$2.0 < y < 2.5$	$2.5 < y < 3.0$	$3.0 < y < 3.5$	$3.5 < y < 4.0$	$4.0 < y < 4.5$
$0-1$	-30.6 ± 0.6	-24.6 ± 0.3	-17.4 ± 0.3	-18.0 ± 0.3	-24.9 ± 0.6
$1-2$	-27.8 ± 0.4	-22.8 ± 0.2	-15.2 ± 0.2	-13.4 ± 0.3	-16.2 ± 0.5
$2-3$	-24.3 ± 0.5	-18.9 ± 0.3	-10.5 ± 0.3	-7.5 ± 0.4	-8.8 ± 0.7
$3-4$	-23.5 ± 0.6	-18.2 ± 0.3	-10.2 ± 0.4	-5.8 ± 0.5	-5.2 ± 0.9
$4-5$	-23.2 ± 0.7	-18.5 ± 0.4	-11.3 ± 0.4	-7.3 ± 0.6	-3.9 ± 1.1
$5-6$	-22.6 ± 0.8	-17.8 ± 0.5	-11.8 ± 0.5	-8.8 ± 0.7	-4.8 ± 1.5
$6-7$	-21.5 ± 1.0	-16.9 ± 0.6	-11.8 ± 0.7	-9.8 ± 1.0	-5.8 ± 1.9
$7-8$	-21.1 ± 1.3	-16.3 ± 0.8	-11.1 ± 0.9	-10.4 ± 1.2	-7.2 ± 2.5
$8-10$	-19.2 ± 1.2	-14.3 ± 0.8	-10.7 ± 1.0	-11.2 ± 1.3	-8.3 ± 2.8
$10-14$	-16.9 ± 1.6	-12.6 ± 1.1	-9.3 ± 1.4	-9.0 ± 2.0	-11.0 ± 4.6
$14-20$	-10.2 ± 1.7 ($2.0 < y < 4.5$)				

Table 20: Relative changes of cross-sections (in %), for a polarisation of $\lambda_\theta = +1$ rather than zero, in (p_{T},y) intervals.

p_{T} [GeV/c]	$2.0 < y < 2.5$	$2.5 < y < 3.0$	$3.0 < y < 3.5$	$3.5 < y < 4.0$	$4.0 < y < 4.5$
$0-1$	28.2 ± 1.2	19.6 ± 0.6	11.8 ± 0.5	12.4 ± 0.5	19.8 ± 1.0
$1-2$	23.9 ± 0.8	17.3 ± 0.4	9.9 ± 0.3	8.4 ± 0.4	10.7 ± 0.7
$2-3$	19.0 ± 0.8	13.1 ± 0.4	6.2 ± 0.4	4.2 ± 0.4	5.1 ± 0.8
$3-4$	18.1 ± 1.0	12.5 ± 0.5	6.1 ± 0.4	3.2 ± 0.5	2.8 ± 1.0
$4-5$	17.7 ± 1.1	12.8 ± 0.6	6.8 ± 0.6	4.1 ± 0.7	2.1 ± 1.2
$5-6$	17.1 ± 1.3	12.2 ± 0.8	7.2 ± 0.7	5.1 ± 0.9	2.6 ± 1.6
$6-7$	15.8 ± 1.6	11.3 ± 1.0	7.2 ± 0.9	5.8 ± 1.2	3.2 ± 2.1
$7-8$	15.3 ± 2.0	10.8 ± 1.2	6.7 ± 1.2	6.2 ± 1.6	4.0 ± 2.9
$8-10$	13.4 ± 1.9	9.2 ± 1.2	6.3 ± 1.3	6.6 ± 1.7	4.7 ± 3.2
$10-14$	11.4 ± 2.3	7.8 ± 1.6	5.5 ± 1.8	5.1 ± 2.5	6.5 ± 5.7
$14-20$	6.0 ± 2.1 ($2.0 < y < 4.5$)				

References

[1] C. E. Carlson and R. Suaya, *Hadronic production of J/ψ mesons*, Phys. Rev. **D14** (1976) 3115.

[2] A. Donnachie and P. V. Landshoff, *Production of lepton pairs, J/ψ and charm with hadron beams*, Nucl. Phys. **B112** (1976) 233.

[3] S. D. Ellis, M. B. Einhorn, and C. Quigg, *Comment on hadronic production of psions*, Phys. Rev. Lett. **36** (1976) 1263.

[4] H. Fritzsch, *Producing heavy quark flavors in hadronic collisions: A test of quantum chromodynamics*, Phys. Lett. **B67** (1977) 217.

[5] M. Glück, J. F. Owens, and E. Reya, *Gluon contribution to hadronic J/ψ production*, Phys. Rev. **D17** (1978) 2324.

[6] C.-H. Chang, *Hadronic production of J/ψ associated with a gluon*, Nucl. Phys. **B172** (1980) 425.

[7] R. Baier and R. Rückl, *Hadronic production of J/ψ and Υ: Transverse momentum distributions*, Phys. Lett. **B102** (1981) 364.

[8] G. T. Bodwin, E. Braaten, and G. P. Lepage, *Rigorous QCD analysis of inclusive annihilation and production of heavy quarkonium*, Phys. Rev. **D51** (1995) 1125, arXiv:hep-ph/9407339.

[9] P. L. Cho and A. K. Leibovich, *Color octet quarkonia production*, Phys. Rev. **D53** (1996) 150, arXiv:hep-ph/9505329.

[10] P. L. Cho and A. K. Leibovich, *Color octet quarkonia production. 2.*, Phys. Rev. **D53** (1996) 6203, arXiv:hep-ph/9511315.

[11] LHCb collaboration, R. Aaij *et al.*, *Measurement of J/ψ production in pp collisions at √s = 2.76 TeV*, JHEP **02** (2013) 041, arXiv:1212.1045.

[12] LHCb collaboration, R. Aaij *et al.*, *Measurement of J/ψ production in pp collisions at √s = 7 TeV*, Eur. Phys. J. **C71** (2011) 1645, arXiv:1103.0423.

[13] LHCb collaboration, R. Aaij *et al.*, *Production of J/ψ and Υ mesons in pp collisions at √s = 8 TeV*, JHEP **06** (2013) 064, arXiv:1304.6977.

[14] LHCb collaboration, R. Aaij *et al.*, *Measurement of forward J/ψ production cross-sections in pp collisions at √s = 13 TeV*, JHEP **10** (2015) 172, Erratum ibid. **05** (2017) 063, arXiv:1509.00771.

[15] ATLAS collaboration, M. Aaboud *et al.*, *Measurement of quarkonium production in proton–lead and proton–proton collisions at 5.02 TeV with the ATLAS detector*, Eur. Phys. J. **C78** (2018) 171, arXiv:1709.03089.

[16] ATLAS collaboration, G. Aad *et al.*, *Measurement of the differential cross-sections of prompt and non-prompt production of J/ψ and ψ(2S) in pp collisions at √s = 7 and 8 TeV with the ATLAS detector*, Eur. Phys. J. **C76** (2016) 283, arXiv:1512.03657.

[17] ATLAS collaboration, T. Zakareishvili, *Measurement of the production cross-section of J/ψ and ψ(2S) mesons at high transverse momentum in pp collisions at $\sqrt{s} = 13$ TeV with the ATLAS detector*, J. Phys. Conf. Ser. **1690** (2020) 012160.

[18] CMS collaboration, A. M. Sirunyan *et al.*, *Measurement of prompt and nonprompt J/ψ production in pp and pPb collisions at $\sqrt{s_{NN}} = 5.02$ TeV*, Eur. Phys. J. **C77** (2017) 269, arXiv:1702.01462.

[19] CMS collaboration, V. Khachatryan *et al.*, *Prompt and non-prompt J/ψ production in pp collisions at $\sqrt{s} = 7$ TeV*, Eur. Phys. J. **C71** (2011) 1575, arXiv:1011.4193.

[20] CMS collaboration, S. Chatrchyan *et al.*, *J/ψ and ψ(2S) production in pp collisions at $\sqrt{s} = 7$ TeV*, JHEP **02** (2012) 011, arXiv:1111.1557.

[21] CMS collaboration, A. M. Sirunyan *et al.*, *Measurement of quarkonium production cross sections in pp collisions at $\sqrt{s} = 13$ TeV*, Phys. Lett. **B780** (2018) 251, arXiv:1710.11002.

[22] ALICE collaboration, B. Abelev *et al.*, *Measurement of prompt J/ψ and beauty hadron production cross sections at mid-rapidity in pp collisions at $\sqrt{s} = 7$ TeV*, JHEP **11** (2012) 065, arXiv:1205.5880.

[23] ALICE collaboration, B. Abelev *et al.*, *Inclusive J/ψ production in pp collisions at $\sqrt{s} = 2.76$ TeV*, Phys. Lett. **B718** (2012) 295, arXiv:1203.3641.

[24] ALICE collaboration, J. Adam *et al.*, *J/ψ suppression at forward rapidity in Pb-Pb collisions at $\sqrt{s_{NN}} = 5.02$ TeV*, Phys. Lett. **B766** (2017) 212, arXiv:1606.08197.

[25] ALICE collaboration, S. Acharya *et al.*, *Inclusive J/ψ production at mid-rapidity in pp collisions at $\sqrt{s} = 5.02$ TeV*, JHEP **10** (2019) 084, arXiv:1905.07211.

[26] ALICE collaboration, K. Aamodt *et al.*, *Rapidity and transverse momentum dependence of inclusive J/ψ production in pp collisions at $\sqrt{s} = 7$ TeV*, Phys. Lett. **B704** (2011) 442, arXiv:1105.0380.

[27] ALICE collaboration, J. Adam *et al.*, *Inclusive quarkonium production at forward rapidity in pp collisions at $\sqrt{s} = 8$ TeV*, Eur. Phys. J. **C76** (2016) 184, arXiv:1509.08258.

[28] ALICE collaboration, S. Acharya *et al.*, *Energy dependence of forward-rapidity J/ψ and ψ(2S) production in pp collisions at the LHC*, Eur. Phys. J. **C77** (2017) 392, arXiv:1702.00557.

[29] CDF collaboration, F. Abe *et al.*, *J/ψ and ψ(2S) production in p$\bar{p}$ collisions at $\sqrt{s} = 1.8$ TeV*, Phys. Rev. Lett. **79** (1997) 572.

[30] CDF collaboration, D. Acosta *et al.*, *Measurement of the J/ψ meson and b−hadron production cross sections in p$\bar{p}$ collisions at $\sqrt{s} = 1960$ GeV*, Phys. Rev. **D71** (2005) 032001, arXiv:hep-ex/0412071.

[31] D0 collaboration, S. Abachi *et al.*, *J/ψ production in p$\bar{p}$ collisions at $\sqrt{s}s = 1.8$ TeV*, Phys. Lett. **B370** (1996) 239.

[32] D0 collaboration, B. Abbott *et al.*, *Small angle J/ψ production in pp̄ collisions at* $\sqrt{s}$ = 1.8 *TeV*, Phys. Rev. Lett. **82** (1999) 35, `arXiv:hep-ex/9807029`.

[33] LHCb collaboration, R. Aaij *et al.*, *Precision luminosity measurements at LHCb*, JINST **9** (2014) P12005, `arXiv:1410.0149`.

[34] LHCb collaboration, R. Aaij *et al.*, *Study of J/ψ production and cold nuclear matter effects in pPb collisions at* $\sqrt{s_{NN}}$ =5 *TeV*, JHEP **02** (2014) 072, `arXiv:1308.6729`.

[35] LHCb collaboration, A. A. Alves Jr. *et al.*, *The LHCb detector at the LHC*, JINST **3** (2008) S08005.

[36] LHCb collaboration, R. Aaij *et al.*, *LHCb detector performance*, Int. J. Mod. Phys. **A30** (2015) 1530022, `arXiv:1412.6352`.

[37] T. Sjöstrand, S. Mrenna, and P. Skands, *A brief introduction to PYTHIA 8.1*, Comput. Phys. Commun. **178** (2008) 852, `arXiv:0710.3820`.

[38] T. Sjöstrand, S. Mrenna, and P. Skands, *PYTHIA 6.4 physics and manual*, JHEP **05** (2006) 026, `arXiv:hep-ph/0603175`.

[39] I. Belyaev *et al.*, *Handling of the generation of primary events in Gauss, the LHCb simulation framework*, J. Phys. Conf. Ser. **331** (2011) 032047.

[40] M. Bargiotti and V. Vagnoni, *Heavy quarkonia sector in PYTHIA 6.324: Tuning, validation and perspectives at LHC(b)*, CERN-LHCB-2007-042, 2007.

[41] D. J. Lange, *The EvtGen particle decay simulation package*, Nucl. Instrum. Meth. **A462** (2001) 152.

[42] N. Davidson, T. Przedzinski, and Z. Was, *PHOTOS interface in C++: Technical and physics documentation*, Comp. Phys. Comm. **199** (2016) 86, `arXiv:1011.0937`.

[43] Geant4 collaboration, J. Allison *et al.*, *Geant4 developments and applications*, IEEE Trans. Nucl. Sci. **53** (2006) 270.

[44] Geant4 collaboration, S. Agostinelli *et al.*, *Geant4: A simulation toolkit*, Nucl. Instrum. Meth. **A506** (2003) 250.

[45] M. Clemencic *et al.*, *The LHCb simulation application, Gauss: Design, evolution and experience*, J. Phys. Conf. Ser. **331** (2011) 032023.

[46] M. De Cian, S. Farry, P. Seyfert, and S. Stahl, *Fast neural-net based fake track rejection in the LHCb reconstruction*, LHCb-PUB-2017-011, 2017.

[47] Particle Data Group, P. A. Zyla *et al.*, *Review of particle physics*, Prog. Theor. Exp. Phys. **2020** (2020) 083C01.

[48] T. Skwarnicki, *A study of the radiative cascade transitions between the Upsilon-prime and Upsilon resonances*, PhD thesis, Institute of Nuclear Physics, Krakow, 1986, DESY-F31-86-02.

[49] K. S. Cranmer, *Kernel estimation in high-energy physics*, Comput. Phys. Commun. **136** (2001) 198, arXiv:hep-ex/0011057.

[50] M. Pivk and F. R. Le Diberder, *sPlot: A statistical tool to unfold data distributions*, Nucl. Instrum. Meth. **A555** (2005) 356, arXiv:physics/0402083.

[51] LHCb collaboration, R. Aaij *et al.*, *Measurement of the track reconstruction efficiency at LHCb*, JINST **10** (2015) P02007, arXiv:1408.1251.

[52] S. Tolk, J. Albrecht, F. Dettori, and A. Pellegrino, *Data driven trigger efficiency determination at LHCb*, LHCb-PUB-2014-039, 2014.

[53] LHCb collaboration, R. Aaij *et al.*, *Measurement of J/ψ polarization in pp collisions at $\sqrt{s} = 7$ TeV*, Eur. Phys. J. **C73** (2013) 2631, arXiv:1307.6379.

[54] Y.-Q. Ma, K. Wang, and K.-T. Chao, *J/ψ(ψ′) production at the Tevatron and LHC at $\mathcal{O}(\alpha_s^4 v^4)$ in nonrelativistic QCD*, Phys. Rev. Lett. **106** (2011) 042002, arXiv:1009.3655.

[55] Y.-Q. Ma and R. Venugopalan, *Comprehensive description of J/ψ production in proton-proton collisions at collider energies*, Phys. Rev. Lett. **113** (2014) 192301, arXiv:1408.4075.

[56] K.-T. Chao *et al.*, *J/ψ polarization at hadron colliders in nonrelativistic QCD*, Phys. Rev. Lett. **108** (2012) 242004, arXiv:1201.2675.

[57] J. L. Albacete, A. Dumitru, H. Fujii, and Y. Nara, *CGC predictions for p + Pb collisions at the LHC*, Nucl. Phys. **A897** (2013) 1, arXiv:1209.2001.

[58] M. Cacciari *et al.*, *Theoretical predictions for charm and bottom production at the LHC*, JHEP **10** (2012) 137, arXiv:1205.6344.

[59] M. Cacciari, M. L. Mangano, and P. Nason, *Gluon PDF constraints from the ratio of forward heavy-quark production at the LHC at $\sqrt{s} = 7$ and 13 TeV*, Eur. Phys. J. **C75** (2015) 610, arXiv:1507.06197.

[60] H. Contopanagos, E. Laenen, and G. F. Sterman, *Sudakov factorization and resummation*, Nucl. Phys. **B484** (1997) 303, arXiv:hep-ph/9604313.

[61] E. G. Ferreiro, F. Fleuret, J. P. Lansberg, and A. Rakotozafindrabe, *Impact of the nuclear modification of the gluon densities on J/ψ production in pPb collisions at $\sqrt{s_{NN}} = 5$ TeV*, Phys. Rev. **C88** (2013) 047901, arXiv:1305.4569.

[62] J. L. Albacete *et al.*, *Predictions for p+Pb collisions at $\sqrt{s_{NN}} = 5$ TeV*, Int. J. Mod. Phys. **E22** (2013) 1330007, arXiv:1301.3395.

[63] F. Arleo and S. Peigné, *J/ψ suppression in p-A collisions from parton energy loss in cold QCD matter*, Phys. Rev. Lett. **109** (2012) 122301, arXiv:1204.4609.

[64] F. Arleo and S. Peigné, *Heavy-quarkonium suppression in p-A collisions from parton energy loss in cold QCD matter*, JHEP **03** (2013) 122, arXiv:1212.0434.

[65] ALICE collaboration, B. Abelev *et al.*, *J/ψ polarization in pp collisions at* $\sqrt{s} = 7$ *TeV*, Phys. Rev. Lett. **108** (2012) 082001, `arXiv:1111.1630`.

[66] CMS collaboration, S. Chatrchyan *et al.*, *Measurement of the prompt J/ψ and* $\psi(2S)$ *polarizations in pp collisions at* $\sqrt{s} = 7$ *TeV*, Phys. Lett. **B727** (2013) 381, `arXiv:1307.6070`.

LHCb collaboration

R. Aaij[32], A.S.W. Abdelmotteleb[56], C. Abellán Beteta[50], T. Ackernley[60], B. Adeva[46],
M. Adinolfi[54], H. Afsharnia[9], C. Agapopoulou[13], C.A. Aidala[86], S. Aiola[25], Z. Ajaltouni[9],
S. Akar[65], J. Albrecht[15], F. Alessio[48], M. Alexander[59], A. Alfonso Albero[45], Z. Aliouche[62],
G. Alkhazov[38], P. Alvarez Cartelle[55], S. Amato[2], J.L. Amey[54], Y. Amhis[11], L. An[48],
L. Anderlini[22], A. Andreianov[38], M. Andreotti[21], F. Archilli[17], A. Artamonov[44], M. Artuso[68],
K. Arzymatov[42], E. Aslanides[10], M. Atzeni[50], B. Audurier[12], S. Bachmann[17], M. Bachmayer[49],
J.J. Back[56], P. Baladron Rodriguez[46], V. Balagura[12], W. Baldini[21], J. Baptista Leite[1],
M. Barbetti[22], R.J. Barlow[62], S. Barsuk[11], W. Barter[61], M. Bartolini[24,h], F. Baryshnikov[83],
J.M. Basels[14], S. Bashir[34], G. Bassi[29], B. Batsukh[68], A. Battig[15], A. Bay[49], A. Beck[56],
M. Becker[15], F. Bedeschi[29], I. Bediaga[1], A. Beiter[68], V. Belavin[42], S. Belin[27], V. Bellee[50],
K. Belous[44], I. Belov[40], I. Belyaev[41], G. Bencivenni[23], E. Ben-Haim[13], A. Berezhnoy[40],
R. Bernet[50], D. Berninghoff[17], H.C. Bernstein[68], C. Bertella[48], A. Bertolin[28], C. Betancourt[50],
F. Betti[48], Ia. Bezshyiko[50], S. Bhasin[54], J. Bhom[35], L. Bian[73], M.S. Bieker[15], S. Bifani[53],
P. Billoir[13], M. Birch[61], F.C.R. Bishop[55], A. Bitadze[62], A. Bizzeti[22,k], M. Bjørn[63], M.P. Blago[48],
T. Blake[56], F. Blanc[49], S. Blusk[68], D. Bobulska[59], J.A. Boelhauve[15], O. Boente Garcia[46],
T. Boettcher[65], A. Boldyrev[82], A. Bondar[43], N. Bondar[38,48], S. Borghi[62], M. Borisyak[42],
M. Borsato[17], J.T. Borsuk[35], S.A. Bouchiba[49], T.J.V. Bowcock[60], A. Boyer[48], C. Bozzi[21],
M.J. Bradley[61], S. Braun[66], A. Brea Rodriguez[46], M. Brodski[48], J. Brodzicka[35],
A. Brossa Gonzalo[56], D. Brundu[27], A. Buonaura[50], L. Buonincontri[28], A.T. Burke[62], C. Burr[48],
A. Bursche[72], A. Butkevich[39], J.S. Butter[32], J. Buytaert[48], W. Byczynski[48], S. Cadeddu[27],
H. Cai[73], R. Calabrese[21,f], L. Calefice[15,13], L. Calero Diaz[23], S. Cali[23], R. Calladine[53],
M. Calvi[26,j], M. Calvo Gomez[85], P. Camargo Magalhaes[54], P. Campana[23],
A.F. Campoverde Quezada[6], S. Capelli[26,j], L. Capriotti[20,d], A. Carbone[20,d], G. Carboni[31],
R. Cardinale[24,h], A. Cardini[27], I. Carli[4], P. Carniti[26,j], L. Carus[14], K. Carvalho Akiba[32],
A. Casais Vidal[46], G. Casse[60], M. Cattaneo[48], G. Cavallero[48], S. Celani[49], J. Cerasoli[10],
D. Cervenkov[63], A.J. Chadwick[60], M.G. Chapman[54], M. Charles[13], Ph. Charpentier[48],
G. Chatzikonstantinidis[53], C.A. Chavez Barajas[60], M. Chefdeville[8], C. Chen[3], S. Chen[4],
A. Chernov[35], V. Chobanova[46], S. Cholak[49], M. Chrzaszcz[35], A. Chubykin[38], V. Chulikov[38],
P. Ciambrone[23], M.F. Cicala[56], X. Cid Vidal[46], G. Ciezarek[48], P.E.L. Clarke[58], M. Clemencic[48],
H.V. Cliff[55], J. Closier[48], J.L. Cobbledick[62], V. Coco[48], J.A.B. Coelho[11], J. Cogan[10],
E. Cogneras[9], L. Cojocariu[37], P. Collins[48], T. Colombo[48], L. Congedo[19,c], A. Contu[27],
N. Cooke[53], G. Coombs[59], I. Corredoira [46], G. Corti[48], C.M. Costa Sobral[56], B. Couturier[48],
D.C. Craik[64], J. Crkovská[67], M. Cruz Torres[1], R. Currie[58], C.L. Da Silva[67], S. Dadabaev[83],
L. Dai[71], E. Dall'Occo[15], J. Dalseno[46], C. D'Ambrosio[48], A. Danilina[41], P. d'Argent[48],
J.E. Davies[62], A. Davis[62], O. De Aguiar Francisco[62], K. De Bruyn[79], S. De Capua[62],
M. De Cian[49], J.M. De Miranda[1], L. De Paula[2], M. De Serio[19,c], D. De Simone[50],
P. De Simone[23], J.A. de Vries[80], C.T. Dean[67], D. Decamp[8], V. Dedu[10], L. Del Buono[13],
B. Delaney[55], H.-P. Dembinski[15], A. Dendek[34], V. Denysenko[50], D. Derkach[82], O. Deschamps[9],
F. Desse[11], F. Dettori[27,e], B. Dey[77], A. Di Cicco[23], P. Di Nezza[23], S. Didenko[83],
L. Dieste Maronas[46], H. Dijkstra[48], V. Dobishuk[52], C. Dong[3], A.M. Donohoe[18], F. Dordei[27],
A.C. dos Reis[1], L. Douglas[59], A. Dovbnya[51], A.G. Downes[8], M.W. Dudek[35], L. Dufour[48],
V. Duk[78], P. Durante[48], J.M. Durham[67], D. Dutta[62], A. Dziurda[35], A. Dzyuba[38], S. Easo[57],
U. Egede[69], V. Egorychev[41], S. Eidelman[43,v], S. Eisenhardt[58], S. Ek-In[49], L. Eklund[59,w],
S. Ely[68], A. Ene[37], E. Epple[67], S. Escher[14], J. Eschle[50], S. Esen[13], T. Evans[48], A. Falabella[20],
J. Fan[3], Y. Fan[6], B. Fang[73], S. Farry[60], D. Fazzini[26,j], M. Féo[48], A. Fernandez Prieto[46],
A.D. Fernez[66], F. Ferrari[20,d], L. Ferreira Lopes[49], F. Ferreira Rodrigues[2], S. Ferreres Sole[32],
M. Ferrillo[50], M. Ferro-Luzzi[48], S. Filippov[39], R.A. Fini[19], M. Fiorini[21,f], M. Firlej[34],
K.M. Fischer[63], D.S. Fitzgerald[86], C. Fitzpatrick[62], T. Fiutowski[34], A. Fkiaras[48], F. Fleuret[12],

M. Fontana[13], F. Fontanelli[24,h], R. Forty[48], D. Foulds-Holt[55], V. Franco Lima[60],
M. Franco Sevilla[66], M. Frank[48], E. Franzoso[21], G. Frau[17], C. Frei[48], D.A. Friday[59], J. Fu[25],
Q. Fuehring[15], E. Gabriel[32], T. Gaintseva[42], A. Gallas Torreira[46], D. Galli[20,d], S. Gambetta[58,48],
Y. Gan[3], M. Gandelman[2], P. Gandini[25], Y. Gao[5], M. Garau[27], L.M. Garcia Martin[56],
P. Garcia Moreno[45], J. García Pardiñas[26,j], B. Garcia Plana[46], F.A. Garcia Rosales[12],
L. Garrido[45], C. Gaspar[48], R.E. Geertsema[32], D. Gerick[17], L.L. Gerken[15], E. Gersabeck[62],
M. Gersabeck[62], T. Gershon[56], D. Gerstel[10], Ph. Ghez[8], L. Giambastiani[28], V. Gibson[55],
H.K. Giemza[36], A.L. Gilman[63], M. Giovannetti[23,p], A. Gioventù[46], P. Gironella Gironell[45],
L. Giubega[37], C. Giugliano[21,f,48], K. Gizdov[58], E.L. Gkougkousis[48], V.V. Gligorov[13], C. Göbel[70],
E. Golobardes[85], D. Golubkov[41], A. Golutvin[61,83], A. Gomes[1,a], S. Gomez Fernandez[45],
F. Goncalves Abrantes[63], M. Goncerz[35], G. Gong[3], P. Gorbounov[41], I.V. Gorelov[40], C. Gotti[26],
E. Govorkova[48], J.P. Grabowski[17], T. Grammatico[13], L.A. Granado Cardoso[48], E. Graugés[45],
E. Graverini[49], G. Graziani[22], A. Grecu[37], L.M. Greeven[32], N.A. Grieser[4], L. Grillo[62],
S. Gromov[83], B.R. Gruberg Cazon[63], C. Gu[3], M. Guarise[21], P. A. Günther[17], E. Gushchin[39],
A. Guth[14], Y. Guz[44], T. Gys[48], T. Hadavizadeh[69], G. Haefeli[49], C. Haen[48], J. Haimberger[48],
T. Halewood-leagas[60], P.M. Hamilton[66], J.P. Hammerich[60], Q. Han[7], X. Han[17], T.H. Hancock[63],
S. Hansmann-Menzemer[17], N. Harnew[63], T. Harrison[60], C. Hasse[48], M. Hatch[48], J. He[6,b],
M. Hecker[61], K. Heijhoff[32], K. Heinicke[15], A.M. Hennequin[48], K. Hennessy[60], L. Henry[48],
J. Heuel[14], A. Hicheur[2], D. Hill[49], M. Hilton[62], S.E. Hollitt[15], J. Hu[17], J. Hu[72], W. Hu[7], X. Hu[3],
W. Huang[6], X. Huang[73], W. Hulsbergen[32], R.J. Hunter[56], M. Hushchyn[82], D. Hutchcroft[60],
D. Hynds[32], P. Ibis[15], M. Idzik[34], D. Ilin[38], P. Ilten[65], A. Inglessi[38], A. Ishteev[83], K. Ivshin[38],
R. Jacobsson[48], S. Jakobsen[48], E. Jans[32], B.K. Jashal[47], A. Jawahery[66], V. Jevtic[15], F. Jiang[3],
M. John[63], D. Johnson[48], C.R. Jones[55], T.P. Jones[56], B. Jost[48], N. Jurik[48],
S.H. Kalavan Kadavath[34], S. Kandybei[51], Y. Kang[3], M. Karacson[48], M. Karpov[82], F. Keizer[48],
M. Kenzie[56], T. Ketel[33], B. Khanji[15], A. Kharisova[84], S. Kholodenko[44], T. Kirn[14],
V.S. Kirsebom[49], O. Kitouni[64], S. Klaver[32], N. Kleijne[29], K. Klimaszewski[36], M.R. Kmiec[36],
S. Koliiev[52], A. Kondybayeva[83], A. Konoplyannikov[41], P. Kopciewicz[34], R. Kopecna[17],
P. Koppenburg[32], M. Korolev[40], I. Kostiuk[32,52], O. Kot[52], S. Kotriakhova[21,38], P. Kravchenko[38],
L. Kravchuk[39], R.D. Krawczyk[48], M. Kreps[56], F. Kress[61], S. Kretzschmar[14], P. Krokovny[43,v],
W. Krupa[34], W. Krzemien[36], W. Kucewicz[35,t], M. Kucharczyk[35], V. Kudryavtsev[43,v],
H.S. Kuindersma[32,33], G.J. Kunde[67], T. Kvaratskheliya[41], D. Lacarrere[48], G. Lafferty[62],
A. Lai[27], A. Lampis[27], D. Lancierini[50], J.J. Lane[62], R. Lane[54], G. Lanfranchi[23],
C. Langenbruch[14], J. Langer[15], O. Lantwin[83], T. Latham[56], F. Lazzari[29,q], R. Le Gac[10],
S.H. Lee[86], R. Lefèvre[9], A. Leflat[40], S. Legotin[83], O. Leroy[10], T. Lesiak[35], B. Leverington[17],
H. Li[72], P. Li[17], S. Li[7], Y. Li[4], Y. Li[4], Z. Li[68], X. Liang[68], T. Lin[61], R. Lindner[48], V. Lisovskyi[15],
R. Litvinov[27], G. Liu[72], H. Liu[6], S. Liu[4], A. Lobo Salvia[45], A. Loi[27], J. Lomba Castro[46],
I. Longstaff[59], J.H. Lopes[2], S. Lopez Solino[46], G.H. Lovell[55], Y. Lu[4], C. Lucarelli[22],
D. Lucchesi[28,l], S. Luchuk[39], M. Lucio Martinez[32], V. Lukashenko[32,52], Y. Luo[3], A. Lupato[62],
E. Luppi[21,f], O. Lupton[56], A. Lusiani[29,m], X. Lyu[6], L. Ma[4], R. Ma[6], S. Maccolini[20,d],
F. Machefert[11], F. Maciuc[37], V. Macko[49], P. Mackowiak[15], S. Maddrell-Mander[54],
O. Madejczyk[34], L.R. Madhan Mohan[54], O. Maev[38], A. Maevskiy[82], D. Maisuzenko[38],
M.W. Majewski[34], J.J. Malczewski[35], S. Malde[63], B. Malecki[48], A. Malinin[81], T. Maltsev[43,v],
H. Malygina[17], G. Manca[27,e], G. Mancinelli[10], D. Manuzzi[20,d], D. Marangotto[25,i], J. Maratas[9,s],
J.F. Marchand[8], U. Marconi[20], S. Mariani[22,g], C. Marin Benito[48], M. Marinangeli[49], J. Marks[17],
A.M. Marshall[54], P.J. Marshall[60], G. Martellotti[30], L. Martinazzoli[48,j], M. Martinelli[26,j],
D. Martinez Santos[46], F. Martinez Vidal[47], A. Massafferri[1], M. Materok[14], R. Matev[48],
A. Mathad[50], Z. Mathe[48], V. Matiunin[41], C. Matteuzzi[26], K.R. Mattioli[86], A. Mauri[32],
E. Maurice[12], J. Mauricio[45], M. Mazurek[48], M. McCann[61], L. Mcconnell[18], T.H. Mcgrath[62],
N.T. Mchugh[59], A. McNab[62], R. McNulty[18], J.V. Mead[60], B. Meadows[65], G. Meier[15],
N. Meinert[76], D. Melnychuk[36], S. Meloni[26,j], M. Merk[32,80], A. Merli[25,i], L. Meyer Garcia[2],

M. Mikhasenko[48], D.A. Milanes[74], E. Millard[56], M. Milovanovic[48], M.-N. Minard[8],
A. Minotti[26,j], L. Minzoni[21,f], S.E. Mitchell[58], B. Mitreska[62], D.S. Mitzel[48], A. Mödden [15],
R.A. Mohammed[63], R.D. Moise[61], T. Mombächer[46], I.A. Monroy[74], S. Monteil[9], M. Morandin[28],
G. Morello[23], M.J. Morello[29,m], J. Moron[34], A.B. Morris[75], A.G. Morris[56], R. Mountain[68],
H. Mu[3], F. Muheim[58,48], M. Mulder[48], D. Müller[48], K. Müller[50], C.H. Murphy[63], D. Murray[62],
P. Muzzetto[27,48], P. Naik[54], T. Nakada[49], R. Nandakumar[57], T. Nanut[49], I. Nasteva[2],
M. Needham[58], I. Neri[21], N. Neri[25,i], S. Neubert[75], N. Neufeld[48], R. Newcombe[61],
T.D. Nguyen[49], C. Nguyen-Mau[49,x], E.M. Niel[11], S. Nieswand[14], N. Nikitin[40], N.S. Nolte[64],
C. Normand[8], C. Nunez[86], A. Oblakowska-Mucha[34], V. Obraztsov[44], T. Oeser[14],
D.P. O'Hanlon[54], S. Okamura[21], R. Oldeman[27,e], M.E. Olivares[68], C.J.G. Onderwater[79],
R.H. O'Neil[58], A. Ossowska[35], J.M. Otalora Goicochea[2], T. Ovsiannikova[41], P. Owen[50],
A. Oyanguren[47], K.O. Padeken[75], B. Pagare[56], P.R. Pais[48], T. Pajero[63], A. Palano[19],
M. Palutan[23], Y. Pan[62], G. Panshin[84], A. Papanestis[57], M. Pappagallo[19,c], L.L. Pappalardo[21,f],
C. Pappenheimer[65], W. Parker[66], C. Parkes[62], B. Passalacqua[21], G. Passaleva[22], A. Pastore[19],
M. Patel[61], C. Patrignani[20,d], C.J. Pawley[80], A. Pearce[48], A. Pellegrino[32], M. Pepe Altarelli[48],
S. Perazzini[20], D. Pereima[41], A. Pereiro Castro[46], P. Perret[9], M. Petric[59,48], K. Petridis[54],
A. Petrolini[24,h], A. Petrov[81], S. Petrucci[58], M. Petruzzo[25], T.T.H. Pham[68], A. Philippov[42],
L. Pica[29,m], M. Piccini[78], B. Pietrzyk[8], G. Pietrzyk[49], M. Pili[63], D. Pinci[30], F. Pisani[48],
M. Pizzichemi[26,48,j], Resmi P.K[10], V. Placinta[37], J. Plews[53], M. Plo Casasus[46], F. Polci[13],
M. Poli Lener[23], M. Poliakova[68], A. Poluektov[10], N. Polukhina[83,u], I. Polyakov[68], E. Polycarpo[2],
S. Ponce[48], D. Popov[6,48], S. Popov[42], S. Poslavskii[44], K. Prasanth[35], L. Promberger[48],
C. Prouve[46], V. Pugatch[52], V. Puill[11], H. Pullen[63], G. Punzi[29,n], H. Qi[3], W. Qian[6], J. Qin[6],
N. Qin[3], R. Quagliani[13], B. Quintana[8], N.V. Raab[18], R.I. Rabadan Trejo[6], B. Rachwal[34],
J.H. Rademacker[54], M. Rama[29], M. Ramos Pernas[56], M.S. Rangel[2], F. Ratnikov[42,82],
G. Raven[33], M. Reboud[8], F. Redi[49], F. Reiss[62], C. Remon Alepuz[47], Z. Ren[3], V. Renaudin[63],
R. Ribatti[29], S. Ricciardi[57], K. Rinnert[60], P. Robbe[11], G. Robertson[58], A.B. Rodrigues[49],
E. Rodrigues[60], J.A. Rodriguez Lopez[74], E.R.R. Rodriguez Rodriguez[46], A. Rollings[63],
P. Roloff[48], V. Romanovskiy[44], M. Romero Lamas[46], A. Romero Vidal[46], J.D. Roth[86],
M. Rotondo[23], M.S. Rudolph[68], T. Ruf[48], R.A. Ruiz Fernandez[46], J. Ruiz Vidal[47],
A. Ryzhikov[82], J. Ryzka[34], J.J. Saborido Silva[46], N. Sagidova[38], N. Sahoo[56], B. Saitta[27,e],
M. Salomoni[48], C. Sanchez Gras[32], R. Santacesaria[30], C. Santamarina Rios[46], M. Santimaria[23],
E. Santovetti[31,p], D. Saranin[83], G. Sarpis[14], M. Sarpis[75], A. Sarti[30], C. Satriano[30,o], A. Satta[31],
M. Saur[15], D. Savrina[41,40], H. Sazak[9], L.G. Scantlebury Smead[63], A. Scarabotto[13], S. Schael[14],
S. Scherl[60], M. Schiller[59], H. Schindler[48], M. Schmelling[16], B. Schmidt[48], S. Schmitt[14],
O. Schneider[49], A. Schopper[48], M. Schubiger[32], S. Schulte[49], M.H. Schune[11], R. Schwemmer[48],
B. Sciascia[23], S. Sellam[46], A. Semennikov[41], M. Senghi Soares[33], A. Sergi[24,h], N. Serra[50],
L. Sestini[28], A. Seuthe[15], Y. Shang[5], D.M. Shangase[86], M. Shapkin[44], I. Shchemerov[83],
L. Shchutska[49], T. Shears[60], L. Shekhtman[43,v], Z. Shen[5], V. Shevchenko[81], E.B. Shields[26,j],
Y. Shimizu[11], E. Shmanin[83], J.D. Shupperd[68], B.G. Siddi[21], R. Silva Coutinho[50], G. Simi[28],
S. Simone[19,c], N. Skidmore[62], T. Skwarnicki[68], M.W. Slater[53], I. Slazyk[21,f], J.C. Smallwood[63],
J.G. Smeaton[55], A. Smetkina[41], E. Smith[50], M. Smith[61], A. Snoch[32], M. Soares[20],
L. Soares Lavra[9], M.D. Sokoloff[65], F.J.P. Soler[59], A. Solovev[38], I. Solovyev[38],
F.L. Souza De Almeida[2], B. Souza De Paula[2], B. Spaan[15], E. Spadaro Norella[25,i], P. Spradlin[59],
F. Stagni[48], M. Stahl[65], S. Stahl[48], S. Stanislaus[63], O. Steinkamp[50,83], O. Stenyakin[44],
H. Stevens[15], S. Stone[68], M.E. Stramaglia[49], M. Straticiuc[37], D. Strekalina[83], F. Suljik[63],
J. Sun[27], L. Sun[73], Y. Sun[66], P. Svihra[62], P.N. Swallow[53], K. Swientek[34], A. Szabelski[36],
T. Szumlak[34], M. Szymanski[48], S. Taneja[62], A.R. Tanner[54], M.D. Tat[63], A. Terentev[83],
F. Teubert[48], E. Thomas[48], D.J.D. Thompson[53], K.A. Thomson[60], V. Tisserand[9],
S. T'Jampens[8], M. Tobin[4], L. Tomassetti[21,f], X. Tong[5], D. Torres Machado[1], D.Y. Tou[13],
M.T. Tran[49], E. Trifonova[83], C. Trippl[49], G. Tuci[29,n], A. Tully[49], N. Tuning[32,48], A. Ukleja[36],

D.J. Unverzagt[17], E. Ursov[83], A. Usachov[32], A. Ustyuzhanin[42,82], U. Uwer[17], A. Vagner[84],
V. Vagnoni[20], A. Valassi[48], G. Valenti[20], N. Valls Canudas[85], M. van Beuzekom[32],
M. Van Dijk[49], E. van Herwijnen[83], C.B. Van Hulse[18], M. van Veghel[79], R. Vazquez Gomez[45],
P. Vazquez Regueiro[46], C. Vázquez Sierra[48], S. Vecchi[21], J.J. Velthuis[54], M. Veltri[22,r],
A. Venkateswaran[68], M. Veronesi[32], M. Vesterinen[56], D. Vieira[65], M. Vieites Diaz[49],
H. Viemann[76], X. Vilasis-Cardona[85], E. Vilella Figueras[60], A. Villa[20], P. Vincent[13],
F.C. Volle[11], D. Vom Bruch[10], A. Vorobyev[38], V. Vorobyev[43,v], N. Voropaev[38], K. Vos[80],
R. Waldi[17], J. Walsh[29], C. Wang[17], J. Wang[5], J. Wang[4], J. Wang[3], J. Wang[73], M. Wang[3],
R. Wang[54], Y. Wang[7], Z. Wang[50], Z. Wang[3], J.A. Ward[56], H.M. Wark[60], N.K. Watson[53],
S.G. Weber[13], D. Websdale[61], C. Weisser[64], B.D.C. Westhenry[54], D.J. White[62],
M. Whitehead[54], A.R. Wiederhold[56], D. Wiedner[15], G. Wilkinson[63], M. Wilkinson[68],
I. Williams[55], M. Williams[64], M.R.J. Williams[58], F.F. Wilson[57], W. Wislicki[36], M. Witek[35],
L. Witola[17], G. Wormser[11], S.A. Wotton[55], H. Wu[68], K. Wyllie[48], Z. Xiang[6], D. Xiao[7], Y. Xie[7],
A. Xu[5], J. Xu[6], L. Xu[3], M. Xu[7], Q. Xu[6], Z. Xu[5], Z. Xu[6], D. Yang[3], S. Yang[6], Y. Yang[6],
Z. Yang[5], Z. Yang[66], Y. Yao[68], L.E. Yeomans[60], H. Yin[7], J. Yu[71], X. Yuan[68], O. Yushchenko[44],
E. Zaffaroni[49], M. Zavertyaev[16,u], M. Zdybal[35], O. Zenaiev[48], M. Zeng[3], D. Zhang[7], L. Zhang[3],
S. Zhang[71], S. Zhang[5], Y. Zhang[5], Y. Zhang[63], A. Zharkova[83], A. Zhelezov[17], Y. Zheng[6],
T. Zhou[5], X. Zhou[6], Y. Zhou[6], V. Zhovkovska[11], X. Zhu[3], Z. Zhu[6], V. Zhukov[14,40],
J.B. Zonneveld[58], Q. Zou[4], S. Zucchelli[20,d], D. Zuliani[28], G. Zunica[62].

[1]*Centro Brasileiro de Pesquisas Físicas (CBPF), Rio de Janeiro, Brazil*
[2]*Universidade Federal do Rio de Janeiro (UFRJ), Rio de Janeiro, Brazil*
[3]*Center for High Energy Physics, Tsinghua University, Beijing, China*
[4]*Institute Of High Energy Physics (IHEP), Beijing, China*
[5]*School of Physics State Key Laboratory of Nuclear Physics and Technology, Peking University, Beijing, China*
[6]*University of Chinese Academy of Sciences, Beijing, China*
[7]*Institute of Particle Physics, Central China Normal University, Wuhan, Hubei, China*
[8]*Univ. Savoie Mont Blanc, CNRS, IN2P3-LAPP, Annecy, France*
[9]*Université Clermont Auvergne, CNRS/IN2P3, LPC, Clermont-Ferrand, France*
[10]*Aix Marseille Univ, CNRS/IN2P3, CPPM, Marseille, France*
[11]*Université Paris-Saclay, CNRS/IN2P3, IJCLab, Orsay, France*
[12]*Laboratoire Leprince-Ringuet, CNRS/IN2P3, Ecole Polytechnique, Institut Polytechnique de Paris, Palaiseau, France*
[13]*LPNHE, Sorbonne Université, Paris Diderot Sorbonne Paris Cité, CNRS/IN2P3, Paris, France*
[14]*I. Physikalisches Institut, RWTH Aachen University, Aachen, Germany*
[15]*Fakultät Physik, Technische Universität Dortmund, Dortmund, Germany*
[16]*Max-Planck-Institut für Kernphysik (MPIK), Heidelberg, Germany*
[17]*Physikalisches Institut, Ruprecht-Karls-Universität Heidelberg, Heidelberg, Germany*
[18]*School of Physics, University College Dublin, Dublin, Ireland*
[19]*INFN Sezione di Bari, Bari, Italy*
[20]*INFN Sezione di Bologna, Bologna, Italy*
[21]*INFN Sezione di Ferrara, Ferrara, Italy*
[22]*INFN Sezione di Firenze, Firenze, Italy*
[23]*INFN Laboratori Nazionali di Frascati, Frascati, Italy*
[24]*INFN Sezione di Genova, Genova, Italy*
[25]*INFN Sezione di Milano, Milano, Italy*
[26]*INFN Sezione di Milano-Bicocca, Milano, Italy*
[27]*INFN Sezione di Cagliari, Monserrato, Italy*
[28]*Universita degli Studi di Padova, Universita e INFN, Padova, Padova, Italy*
[29]*INFN Sezione di Pisa, Pisa, Italy*
[30]*INFN Sezione di Roma La Sapienza, Roma, Italy*
[31]*INFN Sezione di Roma Tor Vergata, Roma, Italy*
[32]*Nikhef National Institute for Subatomic Physics, Amsterdam, Netherlands*

[33] *Nikhef National Institute for Subatomic Physics and VU University Amsterdam, Amsterdam, Netherlands*

[34] *AGH - University of Science and Technology, Faculty of Physics and Applied Computer Science, Kraków, Poland*

[35] *Henryk Niewodniczanski Institute of Nuclear Physics Polish Academy of Sciences, Kraków, Poland*

[36] *National Center for Nuclear Research (NCBJ), Warsaw, Poland*

[37] *Horia Hulubei National Institute of Physics and Nuclear Engineering, Bucharest-Magurele, Romania*

[38] *Petersburg Nuclear Physics Institute NRC Kurchatov Institute (PNPI NRC KI), Gatchina, Russia*

[39] *Institute for Nuclear Research of the Russian Academy of Sciences (INR RAS), Moscow, Russia*

[40] *Institute of Nuclear Physics, Moscow State University (SINP MSU), Moscow, Russia*

[41] *Institute of Theoretical and Experimental Physics NRC Kurchatov Institute (ITEP NRC KI), Moscow, Russia*

[42] *Yandex School of Data Analysis, Moscow, Russia*

[43] *Budker Institute of Nuclear Physics (SB RAS), Novosibirsk, Russia*

[44] *Institute for High Energy Physics NRC Kurchatov Institute (IHEP NRC KI), Protvino, Russia, Protvino, Russia*

[45] *ICCUB, Universitat de Barcelona, Barcelona, Spain*

[46] *Instituto Galego de Física de Altas Enerxías (IGFAE), Universidade de Santiago de Compostela, Santiago de Compostela, Spain*

[47] *Instituto de Fisica Corpuscular, Centro Mixto Universidad de Valencia - CSIC, Valencia, Spain*

[48] *European Organization for Nuclear Research (CERN), Geneva, Switzerland*

[49] *Institute of Physics, Ecole Polytechnique Fédérale de Lausanne (EPFL), Lausanne, Switzerland*

[50] *Physik-Institut, Universität Zürich, Zürich, Switzerland*

[51] *NSC Kharkiv Institute of Physics and Technology (NSC KIPT), Kharkiv, Ukraine*

[52] *Institute for Nuclear Research of the National Academy of Sciences (KINR), Kyiv, Ukraine*

[53] *University of Birmingham, Birmingham, United Kingdom*

[54] *H.H. Wills Physics Laboratory, University of Bristol, Bristol, United Kingdom*

[55] *Cavendish Laboratory, University of Cambridge, Cambridge, United Kingdom*

[56] *Department of Physics, University of Warwick, Coventry, United Kingdom*

[57] *STFC Rutherford Appleton Laboratory, Didcot, United Kingdom*

[58] *School of Physics and Astronomy, University of Edinburgh, Edinburgh, United Kingdom*

[59] *School of Physics and Astronomy, University of Glasgow, Glasgow, United Kingdom*

[60] *Oliver Lodge Laboratory, University of Liverpool, Liverpool, United Kingdom*

[61] *Imperial College London, London, United Kingdom*

[62] *Department of Physics and Astronomy, University of Manchester, Manchester, United Kingdom*

[63] *Department of Physics, University of Oxford, Oxford, United Kingdom*

[64] *Massachusetts Institute of Technology, Cambridge, MA, United States*

[65] *University of Cincinnati, Cincinnati, OH, United States*

[66] *University of Maryland, College Park, MD, United States*

[67] *Los Alamos National Laboratory (LANL), Los Alamos, United States*

[68] *Syracuse University, Syracuse, NY, United States*

[69] *School of Physics and Astronomy, Monash University, Melbourne, Australia, associated to [56]*

[70] *Pontifícia Universidade Católica do Rio de Janeiro (PUC-Rio), Rio de Janeiro, Brazil, associated to [2]*

[71] *Physics and Micro Electronic College, Hunan University, Changsha City, China, associated to [7]*

[72] *Guangdong Provincial Key Laboratory of Nuclear Science, Guangdong-Hong Kong Joint Laboratory of Quantum Matter, Institute of Quantum Matter, South China Normal University, Guangzhou, China, associated to [3]*

[73] *School of Physics and Technology, Wuhan University, Wuhan, China, associated to [3]*

[74] *Departamento de Fisica , Universidad Nacional de Colombia, Bogota, Colombia, associated to [13]*

[75] *Universität Bonn - Helmholtz-Institut für Strahlen und Kernphysik, Bonn, Germany, associated to [17]*

[76] *Institut für Physik, Universität Rostock, Rostock, Germany, associated to [17]*

[77] *Eotvos Lorand University, Budapest, Hungary, associated to [48]*

[78] *INFN Sezione di Perugia, Perugia, Italy, associated to [21]*

[79] *Van Swinderen Institute, University of Groningen, Groningen, Netherlands, associated to [32]*

[80] *Universiteit Maastricht, Maastricht, Netherlands, associated to [32]*

[81] *National Research Centre Kurchatov Institute, Moscow, Russia, associated to [41]*

[82] *National Research University Higher School of Economics, Moscow, Russia, associated to* [42]

[83] *National University of Science and Technology "MISIS", Moscow, Russia, associated to* [41]

[84] *National Research Tomsk Polytechnic University, Tomsk, Russia, associated to* [41]

[85] *DS4DS, La Salle, Universitat Ramon Llull, Barcelona, Spain, associated to* [45]

[86] *University of Michigan, Ann Arbor, United States, associated to* [68]

[a] *Universidade Federal do Triângulo Mineiro (UFTM), Uberaba-MG, Brazil*

[b] *Hangzhou Institute for Advanced Study, UCAS, Hangzhou, China*

[c] *Università di Bari, Bari, Italy*

[d] *Università di Bologna, Bologna, Italy*

[e] *Università di Cagliari, Cagliari, Italy*

[f] *Università di Ferrara, Ferrara, Italy*

[g] *Università di Firenze, Firenze, Italy*

[h] *Università di Genova, Genova, Italy*

[i] *Università degli Studi di Milano, Milano, Italy*

[j] *Università di Milano Bicocca, Milano, Italy*

[k] *Università di Modena e Reggio Emilia, Modena, Italy*

[l] *Università di Padova, Padova, Italy*

[m] *Scuola Normale Superiore, Pisa, Italy*

[n] *Università di Pisa, Pisa, Italy*

[o] *Università della Basilicata, Potenza, Italy*

[p] *Università di Roma Tor Vergata, Roma, Italy*

[q] *Università di Siena, Siena, Italy*

[r] *Università di Urbino, Urbino, Italy*

[s] *MSU - Iligan Institute of Technology (MSU-IIT), Iligan, Philippines*

[t] *AGH - University of Science and Technology, Faculty of Computer Science, Electronics and Telecommunications, Kraków, Poland*

[u] *P.N. Lebedev Physical Institute, Russian Academy of Science (LPI RAS), Moscow, Russia*

[v] *Novosibirsk State University, Novosibirsk, Russia*

[w] *Department of Physics and Astronomy, Uppsala University, Uppsala, Sweden*

[x] *Hanoi University of Science, Hanoi, Vietnam*